Dissolved organic matter fosters core mercury-methylating microbiome for methylmercury production in paddy soils

Qiang Pu[1], Bo Meng[1], Jen-How Huang[1], Kun Zhang[1,2], Jiang Liu[1], Yurong Liu[3], Mahmoud A. Abdelhafiz[1,2,4], Xinbin Feng[1,2]

[1]State Key Laboratory of Environmental Geochemistry, Institute of Geochemistry, Chinese Academy of Sciences, Guiyang, 550081, China
[2]University of Chinese Academy of Sciences, Beijing, 100049, China
[3]State Key Laboratory of Agricultural Microbiology and College of Resources and Environment, Huazhong Agricultural University, Wuhan 430070, China
[4]Geology Department, Faculty of Science, Al-Azhar University, Assiut 71524, Egypt

Correspondence to: Bo Meng (mengbo@mail.gyig.ac.cn)

Abstract. Methylmercury (MeHg), accumulated in rice grain, is highly toxic for human. Its production is largely driven by microbial methylation in paddy soils; however, dissolved organic matter (DOM) is a critical component for soil biogeochemistry process, yet its interactions with microorganisms involved in MeHg production, remains poorly understood. Here, we conducted *hgcA* gene sequencing and genome-resolved metagenomic analysis to identify core Hg-methylating microbiome and investigate the effect of DOM on core Hg-methylating microbiome in paddy soils across a Hg contamination gradient. In general, the Hg-methylating microbial communities varied largely with the degree of Hg contamination in soils. Surprisingly, a core Hg-methylating microbiome was identified that was exclusively associated with MeHg concentration. The partial Mantel test revealed strong linkages among core Hg-methylating microbiome composition, DOM and MeHg concentration. Structural equation model further indicated that core Hg-methylating microbiome composition significantly impacted soil MeHg concentration, contributing to 89% of the observed variation; while DOM play a crucial in determining core Hg-methylating microbiome composition, accounting for 65%. These results suggested that DOM regulates MeHg production by altering the composition of core Hg-methylating microbiome. The presence of various genes associated with carbon metabolism in the metagenome-assembled genome of core Hg-methylating microorganisms suggests that different DOMs stimulate the activity of core Hg-methylating microorganisms to methylate Hg, which was confirmed by pure incubation experiment with *Geobacter sulfurreducens* PCA (a core Hg-methylating microorganism) amended with natural DOM solution extracted from investigated soils. Overall, DOM simultaneously changes core Hg-methylating microbiome composition and functional activity and thus enhances MeHg production in paddy soils.

Keywords. Rice paddy; Mercury methylator; Methylmercury formation; Core microbiome

Graphical abstract

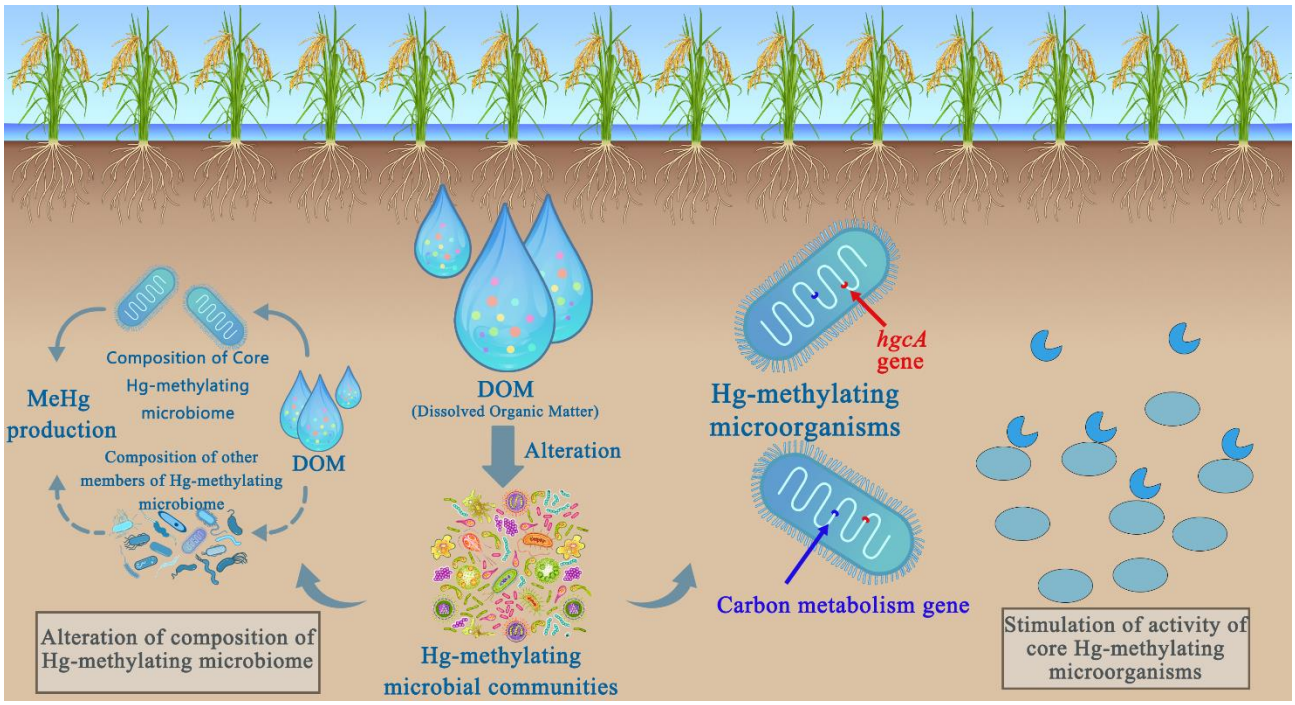

1 Introduction

Mercury (Hg) is a toxic contaminant since it can be transformed into neurotoxic methylmercury (MeHg) and biomagnified in food chains (Driscoll et al., 2013). Human exposure to MeHg can cause neurocognitive deficits and cardiovascular effects (Oulhote et al., 2017; Roman et al., 2011). It is generally accepted that seafood consumption is the major route of exposure to MeHg in humans (Schartup et al., 2019). However, recent studies have demonstrated that rice consumption is another important route of human exposure to MeHg (Feng et al., 2008), as 3.5 billion individuals relying on rice as principal dietary component (Muthayya et al., 2014).

Compared to other environments such as wetlands and aquatic sediments, paddy fields present unique ecological conditions that make them significant hotspots for Hg methylation. The frequent flooding and draining cycles, high organic matter content, and dynamic redox conditions in paddy soils create an environment that supports high levels of microbial activity, particularly Hg-methylating microorganisms (Yin et al., 2013). These conditions not only enhance MeHg production but also increase the likelihood of MeHg entering the food web through rice consumption, posing significant health risks (Zhang et al., 2010). Understanding Hg methylation in paddy fields is therefore crucial, as rice is a critical exposure route for MeHg in humans.

The accumulation of MeHg in rice is mostly attributed to microbial methylation of inorganic Hg in paddy soils (Meng et al., 2011). *In-situ* methylation and demethylation are deemed to be important processes controlling the net MeHg concentration in environments (Barkay and Gu, 2022; Helmrich et al., 2021; Li and Cai, 2012). Our recent study showed that Hg transformation processes, such as methylation, demethylation, oxidation, and reduction, occurred simultaneously in paddy soils, with Hg methylation being the most active (Liu et al., 2023). Therefore, paddy soil is a typical "hotspot" for Hg methylation, which is mainly a biotic process mediated by many abiotic factors, such as Hg bioavailability and redox conditions (Li and Cai, 2012). The diversity and activity of Hg-methylating microorganisms in paddy soils controls MeHg production (Gilmour et al., 2013; Liu et al., 2018). However, among the various Hg-methylating microorganisms currently known, the core microbiome controlling MeHg production and its interaction with environmental variables in paddy soils have yet to be identified.

Physicochemical factors in soils, such as organic matter, pH, salinity, redox potential, iron, and sulfur, have been shown to regulate the activity of Hg-methylating microorganisms and play an important role in controlling MeHg production in rice fields (Ullrich et al., 2001). Among the different variables, soil organic matter, which is ubiquitous in paddy soils (Li et al., 2018), play a vital role in Hg methylation (Yin et al., 2013). Dissolved organic matter (DOM), the most mobile organic matter fraction, increases MeHg production under sulfidic conditions (Graham et al., 2012). DOM increases microbial Hg bioavailability for methylation by stabilizing β-HgS(s) nanoparticles to prevent aggregation. In addition, Hg speciation in Hg-contaminated paddy soils was found to be predominantly regulated by organic matter (Liu et al., 2022), and the high bioavailability of DOM-bound Hg in rice paddies contributed to an increase in MeHg production (Liu et al., 2022). In contrast, other studies reported that DOM had a high affinity for Hg compounds (Skyllberg et al., 2006), suppressing MeHg production due to strong Hg-DOM complexation (Schartup et al., 2015). As a result, the role of paddy soil DOM on Hg methylation remains elusive. Our recent study showed a significant and strong relationship between MeHg production and low-molecular-weight DOMs in paddy soils collected from major rice-producing areas across China (Abdelhafiz et al., 2023). Given paddy soil DOM's significant chemodiversity (Li et al., 2018), it is reasonable to hypothesize that the effect of DOM on MeHg production cannot be assessed solely based on Hg speciation and bioavailability, suggesting that other factors also play roles in MeHg production.

MeHg production is controlled by the synergy of Hg bioavailability and Hg-methylation capacity (Peterson et al., 2023), indicating that Hg-methylating microbial communities may also play an important role in DOM-regulated MeHg production. Concentration and composition of DOM have been shown to regulate MeHg production via alteration of the composition of the soil microbial community (Fagervold et al., 2014; Hu et al., 2021; Oloo et al., 2016). However, the core Hg-methylating microorganisms were not identified within these studies. Zhao et al. (2017) reported that two model Hg methylators exhibited an opposite response to DOM at the strain level. Therefore, we hypothesized that DOM fosters a core Hg-methylating microbiome that regulates MeHg production, since the core microbiome has a pivotal role in the functioning of ecosystems (Banerjee et al., 2018; Chen et al., 2019; Xun et al., 2021).

Thus, an attempt was made within this study to verify the crucial role of DOM in fostering the core Hg-methylating microbiome for MeHg production by (1) identifying the core Hg-methylating microbiome in paddy soils across a gradient of Hg contamination, (2) quantifying the relevance of DOM to core Hg-methylating microbiome and MeHg production in paddy soils compared with other soil physicochemical parameters, and (3) elucidating the mechanism of core Hg-methylating microorganisms in response to different DOMs. These results broaden our understanding of DOM as the prominent factor in altering Hg-methylating microbial communities and highlight the contribution of the core Hg-methylating microbiome to MeHg production in paddy soils.

2 Materials and methods

2.1 Soil sampling and physico-chemical analysis

Two field sampling campaigns were conducted in September 2020 and August 2022 in this study. Specifically, paddy fields from an abandoned Hg mining area (Sikeng, SK), an artisanal Hg smelting area (Gouxi, GX), and a regional background area (Huaxi, HX) in Guizhou Province, SW-China, were selected in September 2020 (Table S1, S1- S27). In each study area (SK, GX, and HX), nine sampling sites were randomly selected. Similarly, additional 19 sampling sites from the rice producing areas in 12 provinces of China were selected in August 2022 (Table S1, S28-S46). At each site, one rice paddy field was randomly selected. Paddy soil was taken from the root zone (10-20 cm deep) and comprised a composite of three subsamples from the same paddy field. A total of 46 soil samples were obtained in this study to represent different Hg contamination levels and bioavailability, net MeHg production, DOM concentration and composition, soil microbial community composition and structure, and other physicochemical characteristics. Soil samples were collected in the sterile PP bottles (Nalgene®, Thermo Fisher, USA) without any headspace, immediately shipped back to the laboratory on ice packs (~4°C) and divided into two subsamples before use. One subsample was stored at -20°C for microbial analysis, and the other was stored at 4°C for the analysis of soil physicochemical properties. Freeze-dried samples (-80 ºC; Eyela FDU-2110, China) were screened to remove gravel and residue, then ground and evenly mixed using a mortar and pestle to pass through a 200-mesh sieve. The processed soil samples were analysed for pH, total carbon (TC), total nitrogen (TN), and various mercury species (water-soluble Hg, total Hg (THg), and MeHg), water-soluble sulfate (SO_4^{2-}) and nitrate (NO_3^-), DOM concentration (measured as water-soluble dissolved organic carbon), DOM composition (measured as optical properties of DOM) and low-molecular-weight organic acids. Fresh soil samples were also centrifuged to obtain pore water for the analysis of iron and sulfur (measured as Fe^{2+} and S^{2-} in soil pore water). Detailed measurement procedures are provided in Supplementary Text S1. It should be noted that Fe^{2+} and S^{2-}data were limited to soil samples obtained in August 2022.

2.2 Soil DNA extraction

We extracted DNA from 0.5 g of soil using the FastDNA Spin Kit for Soil (MP Biomedicals, France), following the manufacturer's instructions. The quality and concentration of the isolated DNA were assessed using spectrophotometry (Nanodrop ND1000, USA) and 1.0% agarose gel electrophoresis. The DNA was then stored at -80 ºC for further analysis.

2.3 Amplicon sequencing and bioinformatic analysis

Soil Hg-methylating microbial communities were characterized by Illumina MiSeq sequencing of the *hgcA* gene using the primer pair ORNL-HgcAB-uni-F (5'-AAYGTCTGGTGYGCNGCVGG-3′) and the reverse primer ORNL-HgcAB-uni-32R (5'-CAGGCNCCGCAYTCSATRCA-3′) (Gionfriddo et al., 2020). Amplicons were equimolarly mixed, and sequenced using the Illumina MiSeq instrument (Illumina Inc., San Diego) in 2×300 bp mode. Poor-quality reads, adapters and primers were trimmed with SICKLE and CUTADAPT (Joshi and Fass, 2011; Martin, 2011). USEARCH (version 8.0) was used to truncate, dereplicate, sort and remove singletons (Edgar, 2013). The set of sequences obtained was clustered at a 60% similarity cutoff with cd-hit-est (Fu et al., 2012). Using USEARCH (version 8.0), the sequences were then mapped to the resulting clusters' representative sequences to build a count table. The sequences were annotated with amino acid sequences from Hg-MATE-Db (V1.01142021) (Gionfriddo et al., 2021) by using a Hidden Markov Model (HMM) based on HMMER (Eddy, 2011). In addition, the abundance of the Hg-methylating gene *hgcA* (which encodes a corrinoid protein essential for methylating inorganic Hg) was quantified in an Applied Biosystem 7500. The quantification of the *hgcA* gene is provided in Text S2.

2.4 Metagenomic sequencing and bioinformatic analysis

DNA from nine randomly selected paddy fields at each site in September 2020 was equimolarly mixed to obtain >1 μg of DNA for shotgun metagenomic sequencing. For paddy soils collected in August 2022, three replicates of each sample were utilized to ensure sufficient quantity and quality of DNA for metagenomic sequencing. A total of 22 samples were analysed using an Illumina HiSeq 2500 system (Illumina Corp., USA).

The detection and taxonomic identification of the *hgcAB* gene (full operon responsible for Hg methylation pathway) was performed with marky-coco (Capo et al., 2023). The metagenomic sequences were trimmed to eliminate low-quality reads using fastp with the following parameters: -q 30 -l 25 --detect_adapter_for_pe --trim_poly_g --trim_poly_x (Chen et al., 2018). These high-quality reads were then assembled into contigs using megahit 1.1.2 with default settings (Li et al., 2016). The annotation of the contigs for prokaryotic protein-coding gene prediction was conducted using prodigal 2.6.3 (Hyatt et al., 2010). To search for *hgc* homologs, a profile of HMM derived from Hg-MATE.db.v1 was applied to amino acid FASTA file generated from each assembly with the function hmmsearch from HMMER 3.2.1 (Finn et al., 2011). To eliminate paralogs of *hgcA*, we removed the sequences without the conserved putative cap helix motif [N(V/I)WCA(A/G)GK] reported previously (Parks et al., 2013). We further filtered the sequences by retaining only sequences with more than four transmembrane domains as identified by TMHMM (v.2.0) (Krogh et al., 2001). Finally, the obtained contigs with *hgcA* homologs were classified taxonomically following a previously described method (Zhang et al., 2023). In addition, to estimate the relative abundance of the *hgcA* gene, metagenomic reads were mapped to representative genomes of the *hgcA* dataset using Bowtie2 (Capo et al., 2023). The relative abundances of each gene were calculated by normalizing the total length of successfully mapped reads by gene length and the total number of reads in the metagenome.

Contigs ≥ 1000 bp were used to carry out binning analysis with the MetaWRAP pipeline (v1.3.2) (Uritskiy et al., 2018). The quality of reconstructed metagenome-assembled genomes (MAGs) was assessed using CheckM (Parks et al., 2015). High-quality MAGs (completeness ≥ 90% and contamination ≤ 10%) were used to detect *hgcA* homologs, and taxonomy

of these retrieved MAGs was conducted using GTDB-tk (v2.1.0) with its reference database (version release_207V2) (Parks et al., 2022). To explore what fractions of DOM can be metabolized by core Hg-methylating microorganisms, core Hg-methylating microbial-associated MAGs were mapped to the protein sequence of the Kyoto Encyclopedia of Genes and Genomes (KEGG) database using eggNOG mapper (Huerta-Cepas et al., 2017).

2.5 Pure incubation of *Geobacter sulfurreducens* PCA with different DOMs

To validate that different concentrations and molecular weights of DOM stimulate the activity of core Hg-methylating microorganisms, we incubated *Geobacter sulfurreducens* PCA (*G. sulfurreducens* PCA), identified as a core Hg-methylating microorganism in this study, with Hg^{2+}, and a natural DOM solution extracted from NMS, MMS, or HMS soils. *Geobacter* was selected for these pure incubation experiments due to its dominant role in mercury methylation and its ability to isolate the effects of DOM on methylation rates without the interference of soil matrix complexity. More details on the descriptions for the pure incubation experiment can be found in Text S3.

2.6 Statistical analysis

Statistical analysis was conducted with SPSS 27 (SPSS, Chicago, IL), AMOS (SPSS, Chicago, IL), and R platform (version 3.6.1). All statistical tests were considered significant at $p < 0.05$. The Kruskal-Wallis test was used to compare microbial alpha diversity among all samples. Hg-methylating microbial communities across differentially-polluted soils were compared by analysing dissimilarity matrices using Bray-Curtis distance and visualized using principal coordinates analysis (PCoA) and Adonis with the "ade4" and "vegan" packages (Dray and Dufour, 2007; Oksanen et al., 2017). To determine the relationship between THg and MeHg, Spearman correlation was performed using "ggpubr" and visualized using "ggplot2" packages (Kassambara, 2018; Wickham, 2009). Variation partitioning analysis was performed using "vegan" package (Oksanen et al., 2017). The major predictors of Hg-methylating microbial communities and their significance were identified using random forest analysis with "randomForest", "rfPermute" and "A3" packages (Archer, 2018; Fortmann-Roe, 2015; Liaw and Wiener, 2002). To investigate the co-occurrence patterns among microbial taxa related to MeHg production, co-occurrence networks were established in the R platform using “psych” package (Revelle, 2023), and visualized in Gephi 0.9.2 (Bastian et al., 2009) based on strong (Spearman’s $r > 0.8$) and significant ($p < 0.01$) correlations (De Caceres and Legendre, 2009). The modules in Hg-methylating microbial network were identified using default parameters from Gephi. To explore the relationship between the modules and environmental parameters, we correlated dissimilarities of bacterial composition in core Hg-methylating microbiome with those of environmental factors as previously described (Sunagawa et al., 2015). The structural equation model (SEM) was conducted using AMOS 28 to evaluate the impacts of DOM and core Hg-methylating microbiome on MeHg production. A *prior* model was established based on the known relationships among drivers impacting MeHg production (Fig. S1). We further calculated the contribution of ecological parameters, including DOM, to the core Hg-methylating microbiome, and the contribution of the core Hg-methylating microbiome to MeHg production, following the approach described by Tao et al. This calculation was performed by determining the proportion of the squared path coefficient of each parameter relative to the sum of the squared path coefficients of all parameters influencing the same target variable (Tao et al., 2015).

3 Results

3.1 Mercury production in paddy soils

THg concentrations in paddy soils ranged from 0.03 to 1079.75 μg/g dw (Table S1). As reported in our previous study, dividing paddy soils by THg concentration rather than sampling sites facilitates a comprehensive investigation of the key

factors influencing Hg methylation (Abdelhafiz et al., 2023). Therefore, the paddy soils in this study were divided into three categories according to THg concentration: non-Hg contaminated soils (NMS, with average levels of 0.24 ± 0.18 μg/g dw, n=23), moderate Hg-contaminated soils (MMS, 18.28 ± 6.77 μg/g dw, n=13), and high Hg-contaminated soils (HMS, 637.79 ± 160.93 μg/g dw, n=10). Furthermore, statistically significant differences in DOM concentrations (reflected by DOC concentration) and DOM composition (reflected by S_R of DOM) were found in NMS, MMS and HMS (Table S2). Specifically, DOC concentration varied significantly across the three soil types, with 0.48 ± 0.13 in NMS, 0.40 ± 0.07 in MMS, and 0.30 ± 0.10in HMS. Similarly, the S_R of DOM differed markedly between NMS (1.40 ± 0.76), MMS (0.89 ± 0.09), and HMS (0.46 ± 0.09). However, no discernible differences in physicochemical properties (e.g., pH, S^{2-}, SO_4^{2-}, NO_3^-, TN, TC, Fe^{2+}) were observed in NMS, MMS and HMS (Table S3).

In this study, we found MeHg concentration in paddy soils in the order of HMS (5.01 ± 0.77 ng/g dw, n=10) ≥ MMS (2.54 ± 0.72 ng/g dw, n=13) > NMS (0.76 ± 0.25 ng/g dw, n=23) (Fig. S2). Accordingly, a positive relationship was observed between total Hg and MeHg in different paddy soils (Fig. S3).

3.2 Core mercury-methylating microbiome as predictors of MeHg production in paddy soils

Random forest result revealed that *hgcA* gene abundance, DOM concentration, DOM composition, water-soluble Hg, Fe^{2+}, and S^{2-} were significantly ($p < 0.05$) associated with MeHg concentration (Fig. S4), with the *hgcA* gene as the strongest predictor. The *hgcA* gene-based taxonomic profiles of paddy soils reveal changes in Hg-methylating microbial community compositions across different levels of Hg pollution (Fig. 1a). Such observations were additionally supported by (1) the Chao1 index revealing the diversity of Hg-methylating microorganisms in the order of MMS (312.57 ± 44.73) > NMS (268.47 ± 81.85) > HMS (187.08 ± 131.62) ($p < 0.05$; Fig. 1b) and (2) the divergent patterns of Hg-methylating microbial communities in paddy soils ($p < 0.01$; Fig. 1c). The shotgun metagenomics results were consistent in detecting Hg-methylating microbial community composition and structure (Fig. S5). *Proteobacteria*, *Acidobacteria*, and *Chloroflexi* were the most abundant phyla in different paddy soils detected by both sequencing strategies. In summary, using both *hgcA* gene sequencing and metagenomic data, a significant difference in Hg-methylating microbial community structure and diversity was observed in paddy soils.

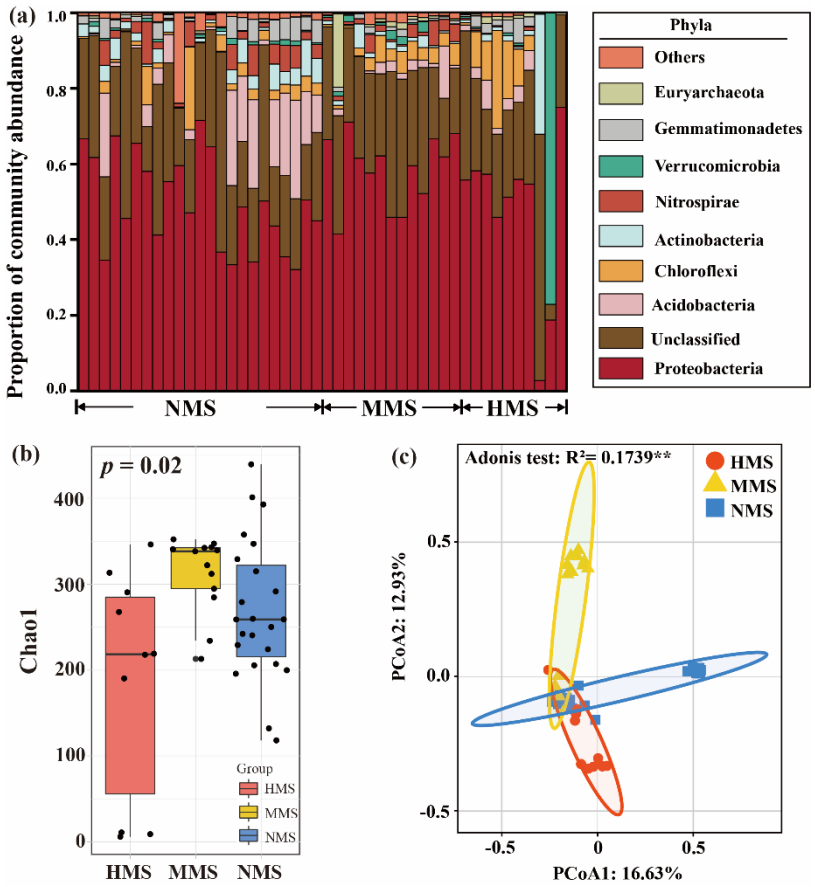

Figure 1: Taxonomic profiles of Hg-methylating microbial communities in paddy soils based on amplicon sequencing. (a) Microbial community composition in differently polluted paddy soils. Phyla with low abundance grouped together under "other phyla". **(b)** Microbial diversity (based on the Chao1 index) in differently polluted paddy soils. **(c)** Principal coordinates analysis (PCoA) based on Bray-curtis distance showing the overall pattern of Hg-methylating microbial communities in differently polluted paddy soils. NMS, non-Hg polluted paddy soils (n = 23); MMS, moderate Hg-polluted paddy soils (n = 13); HMS, high Hg-polluted paddy soils (n = 10).

Network analysis captured six, eleven, and eleven modules (modularity index > 0.55) in NMS, MMS, and HMS, respectively (Fig. 2a, Table S4). Among all modules, Hg-methylating microorganisms in Module1 in NMS, MMS and HMS were identified as core Hg-methylating microbiome based on their (1) higher connections to other modules and (2) higher abundance in total Hg-methylating microbial community (Table S5). Importantly, the impact of various modules in the microbial community on MeHg production was analyzed using random forest analysis. The results revealed that the microbiome in Module 1 is a crucial bacterial group influencing soil methylmercury concentration (Fig. 2b). This group is considered the core Hg-methylating microbiome in this study. Further analysis of the core Hg-methylating microbiome composition revealed diverse core Hg-methylating microorganisms in paddy soils. Although most microorganisms are not annotated, the three genera with the highest abundance in each soil type are as follows: In NMS, *Geobacter* (36.2%), *Syntrophus* (1.7%), *and Desulfomonas* (0.4%) dominate; in MMS, *Geobacter* (40.5%), *Granulicella* (2.9%), and *Olavius* (2.9%) are the most abundant; and in HMS, *Geobacter* (56.8%), *Methanoregula* (0.6%), and *Granulicella* (2.3%) prevail (Fig. 2c). It is worth highlighting that, in this study, microorganisms belonging to *Geobacter* were identified as the most significant core microorganisms for Hg methylation across all paddy soils.

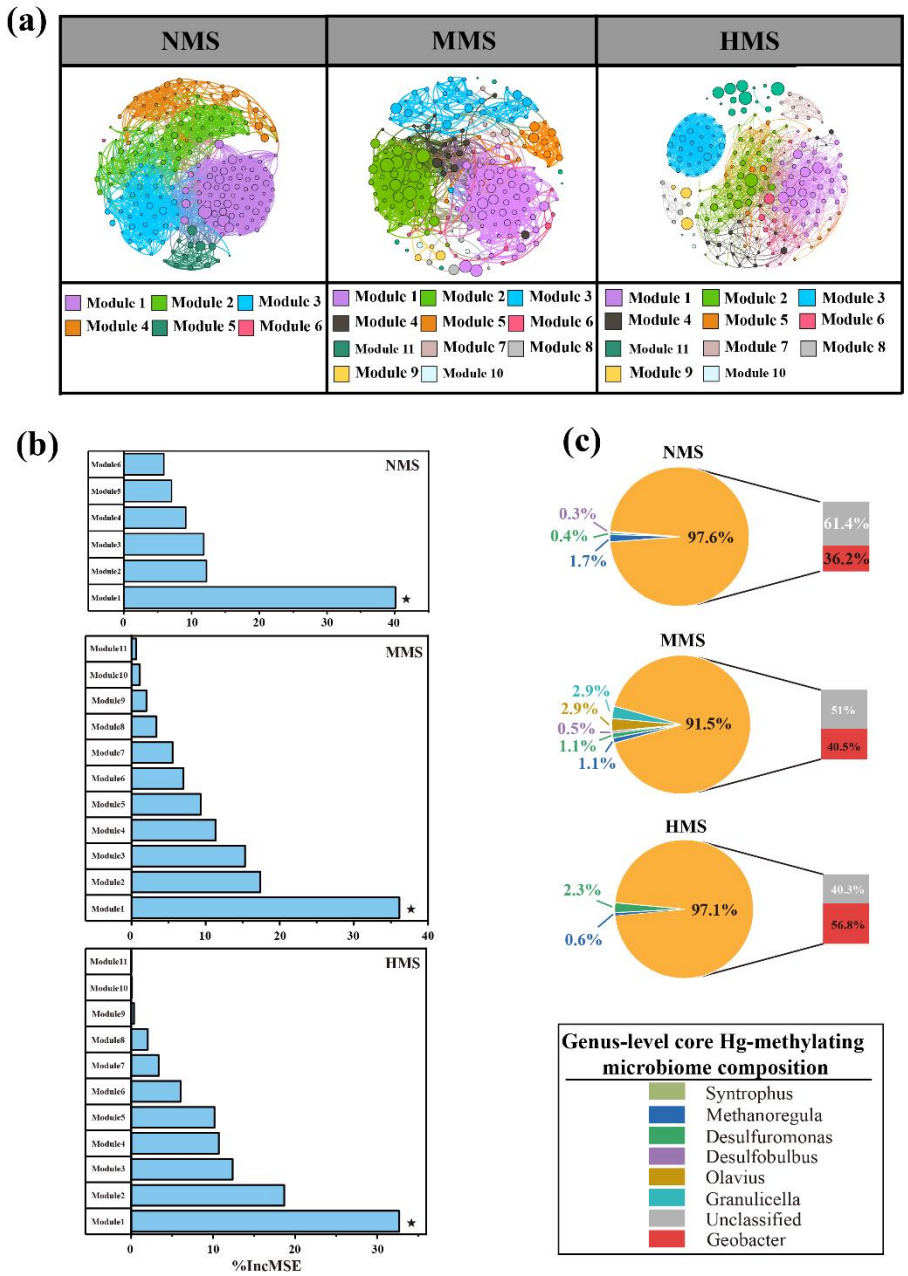

Figure 2: Core Hg-methylating microbiome in paddy soils. (a) Co-occurrence network of Hg-methylating microbial community in differently polluted paddy soils. Each node represents one OTU. The node size is proportional to the relative abundance of OTUs. **(b)** Predictors of the MeHg production in differently polluted paddy soils based on Random Forest analysis. Only predictors with significant effects are labeled asterisks. **(c)** Core Hg-methylating microbiome composition at genus level in differently polluted paddy soils. NMS, non-Hg polluted paddy soils (n = 23); MMS, moderate Hg-polluted paddy soils (n = 13); HMS, high Hg-polluted paddy soils (n = 10).

3.3 Dissolved organic matter as indicators of core mercury-methylating microbiome composition in paddy soils

Based on analysis of correlations, the results showed that there were significant correlations between core Hg-methylating microbiome composition, MeHg concentration, DOM concentration, DOM composition, water-soluble Hg, soil S^{2-} and Fe^{2+} (Fig. 3). Among all parameters, DOM is the most important factor influencing the composition of core Hg-methylating microbiome. This was supported by DOM explaining the most to core Hg-methylating microbiome composition (Fig. S6). Random forest analysis also showed that DOM concentration and composition were the most important predictors of the composition of core Hg-methylating microbiome (Fig. S7). Additionally, SEM result showed that the core Hg-methylating microbiome composition, which is closely linked to *hgcA* gene abundance, significantly regulated soil MeHg concentration ($\lambda = 0.84$, $p < 0.001$) (Fig. 4). In comparison, the contributions of Hg bioavailability

and redox conditions to the core Hg-methylating microbiome composition are 10% and 25%, respectively, which are much lower than that of DOM (65%) (Fig. 4).

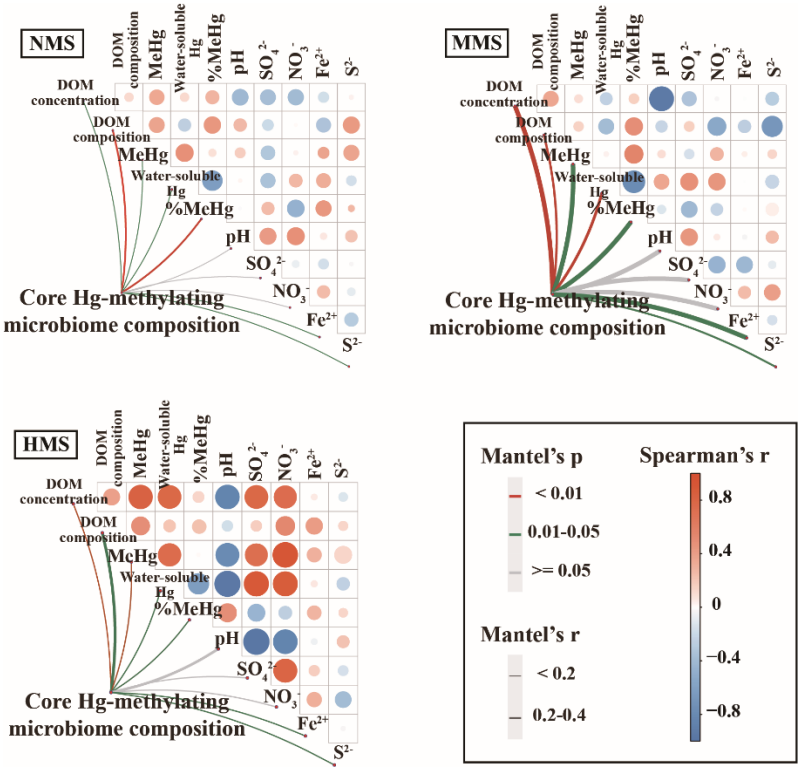

Figure 3. Pairwise comparisons of environmental factors and community taxonomic composition in core Hg-methylating microbiome in differently polluted paddy soils. NMS, non-Hg polluted paddy soils; MMS, moderate Hg-polluted paddy soils; HMS, high Hg-polluted paddy soils.

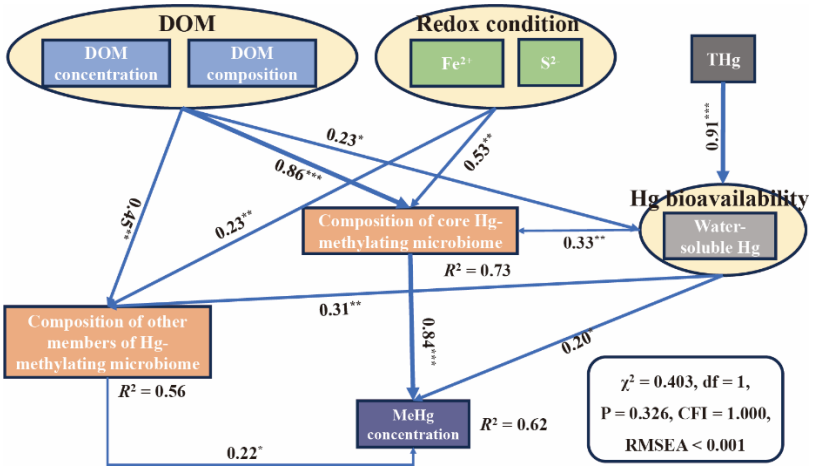

Figure 4. Structural equation models showing the effects of DOM, redox conditions, and Hg bioavailability on MeHg production. NMDS1 values of the NMDS analysis were used for the representation of DOM and Redox condition in the SEMs. Numbers adjacent to arrows are standardized path coefficients, and numbers in brackets denote p values. 'Statistically nonsignificant' results are not shown in the figure. R^2 denotes the proportion of variance explained.

3.4 Dissolved organic matter stimulates activity of core mercury-methylating microorganism enhancing methylmercury production in paddy soils

The results of metagenomic-binning revealed that three core Hg-methylating microbial-associated metagenome-assembled genomes (MAGs, completeness ≥ 90% and contamination ≤ 10%) carried different carbon utilization genes (*ackA*, *sdhA*, or *ppdK* gene) (Fig. 5), which are responsible for acetate kinase, succinate dehydrogenase, pyruvate and

orthophosphate dikinase. These results indicated that the low-molecular-weight DOMs in soil selectively stimulate the activity of core Hg-methylating microorganism that preferentially utilize them for metabolism, leading to the increase of MeHg concentration.

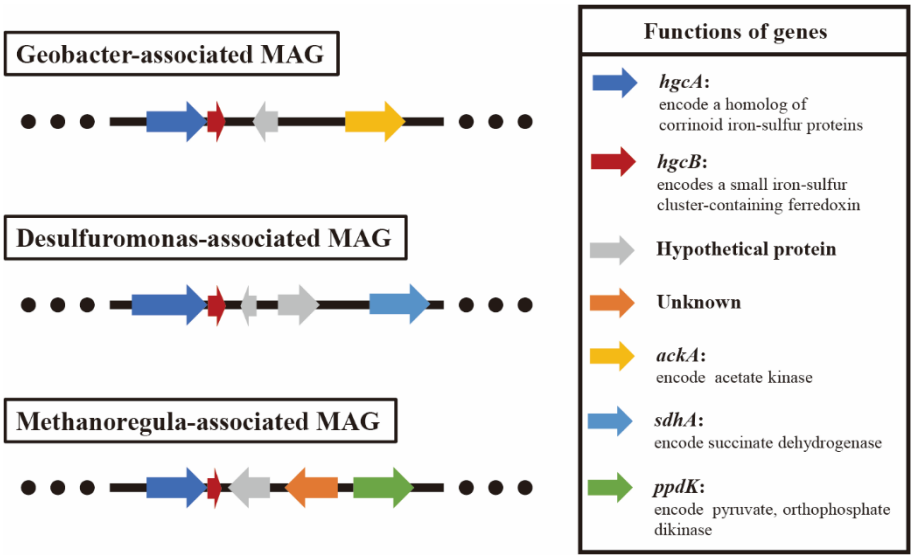

Figure 5. Analysis of the genetic context of *hgcA* gene and genes involved in carbon metabolism in core Hg-methylating microbial-associated MAGs. The extents and directions of genes are shown by arrows labeled with gene names.

To validate this hypothesis, *Geobacter sulfurreducens* PCA, core Hg-methylating microorganism identified in this study, was incubated with $HgCl_2$ and various DOM solutions extracted from investigated paddy soils. The results showed distinct patterns in MeHg production (Fig. 6), confirming that different concentration of low-molecular-weight DOMs significantly regulates MeHg production by influencing the activity of core Hg-methylating microorganisms.

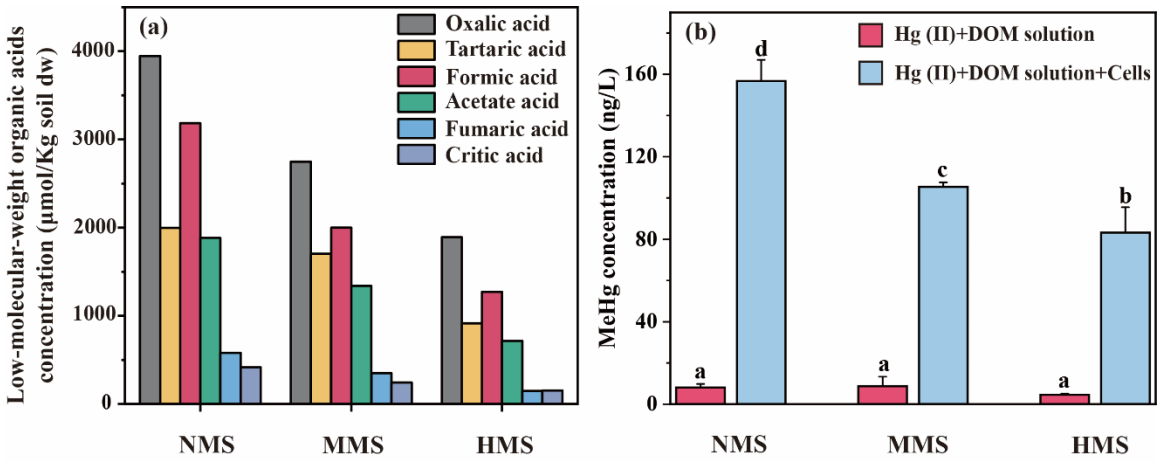

Figure 6. Effect of natural DOM solution extracted from paddy soils on MeHg production by core Hg methylator (*Geobacter sulfurreducens* PCA). (a) The concentration of low-molecular-weight organic acids in paddy soils from non-Hg polluted soils (NMS), moderate Hg-polluted soils (MMS) and high Hg-polluted soils (HMS). **(b)** MeHg concentration by *G. sulfurreducens* PCA. Data (n = 3) are presented as mean value ± SD, with error bars representing standard deviations. Significant differences among different treatments were tested with Tukey's honest significance test; different lowercase letters in each bar indicate significant differences among treatments ($p < 0.05$).

4 Discussion

Our study found that MeHg concentration was strongly linked to *hgcA* gene abundance even compared to abiotic factors, which suggested that MeHg production is a microbially-mediated process (Parks et al., 2013; Podar et al., 2015). Our study further revealed that although there are significant differences in the Hg-methylating microbial communities in different polluted paddy soils, they all have a core Hg-methylating microbiome, which plays a more important role than

other Hg methylators in regulating MeHg production. As illustrated by a previous study, the major module (also known as the core microbiome) in microbial community network contributes to the stability of soil microbiome, enhancing its resistance to climate changes and nutrient fertilization (Jiao et al., 2022). These findings establish the presence of a major module contributing exclusively to Hg methylation in paddy soils, although there are many more Hg-methylating microorganisms present. In fact, microorganisms containing the *hgcA* gene are able to methylate Hg, but this does not mean that they are automatically active in Hg methylation.

The SEM analysis result indicated that although redox conditions and Hg bioavailability significantly affected the composition of core Hg-methylating microbiome, their contribution to the composition of core Hg-methylating microbiome was less and weaker than that of DOM. The explanation for this phenomenon may be that (1) the soil collected in the paddy field during the flooding period is in an anaerobic state, so the selection of redox conditions on core mercury-methylating microorganisms is weakened; (2) Hg is a toxic element to microorganisms and is usually not involved in microbial metabolism (Wang et al., 2020). Environmental Hg may induce the persistence of some microorganisms. Therefore, long-term Hg contamination often only elevates the abundance of specific microbial taxa capable of Hg tolerance (Frossard et al., 2018); (3) DOM, an important carbon source and nutrient in nature, is involved in microbial respiration and metabolism (Kujawinski, 2011). Consequently, the concentration and composition of DOM contributed significantly to core Hg-methylating microbiome. These results highlight the dominant role of DOM in shaping core Hg-methylating communities, as compared to redox conditions and Hg bioavailability.

Our study found that *Geobacter*, *Desulfuromonas*, and *Methanoregular*, *Syntrophus*, *Granulicella*, and *Olavius* are core Hg-methylating microorganisms in paddy soils. Previous studies confirmed that *Geobacter*, *Desulfuromonas*, and *Syntrophus* have the capability for Hg methylation (Bravo et al., 2018; Gilmour et al., 2013; Liu et al., 2018; Zhong et al., 2024). In addition, *Methanoregular* spp., as methanogenic archaea, show potential for Hg methylation (Jones et al., 2019). *Granulicella* affects the decomposition of complex organic materials (Pankratov and Dedysh, 2010), while *Olavius* plays a role in sulfur and nitrogen cycling (Blazejak et al., 2005). These roles suggest that both microorganisms could also be important potential Hg methylators. Although many core Hg-methylating microorganisms have not been annotated, our study emphasizes that the annotated Hg-methylating microorganisms play a much greater role in Hg methylation in paddy soils than previously thought.

Our study identified various DOMs components, including oxalic acid, tartaric acid, formic acid, acetate acid, fumaric acid, and citric acid, in paddy soils. These low-molecular-weight organic acids, particularly abundant in NMS soils, serve as key carbon sources for Hg-methylating microorganisms and stimulate the growth and activity of the core Hg-methylating microbiome. Pure incubation of *Geobacter sulfurreducens* PCA (core Hg-methylating microorganism identified in our paddy soils) further confirmed that different concentration of low-molecular-weight DOM solution extracted from natural paddy soils obtained from NMS, MMS and HMS had significant effects on MeHg concentration. These findings demonstrate that DOM composition strongly influences microbial Hg methylation by stimulating key metabolic pathways. For instance, *Geobacter sulfurreducens* and *Desulfovibrio desulfuricans* use acetate and fumarate in the TCA cycle, supporting anaerobic respiration and electron transport that enhance Hg methylation (Hu et al., 2013; Liu et al., 2018). Similarly, methanogenic archaea such as *Methanoregula* and *Methanosarcina* utilize formate and acetate through methanogenesis, further contributing to Hg methylation (Sakai et al., 2010; Schöne et al., 2022). Although metabolomic data were not included in this study, future research incorporating such analyses could provide valuable insights into how specific DOM components influence microbial metabolism and Hg methylation, revealing key metabolites and pathways such as acetate fermentation, methanogenesis, and electron transfer processes. This highlights how specific DOM components shape the core Hg-methylating microbiome and influence its role in MeHg production.

In contrast to low-molecular-weight organic acids, other DOM components such as aromatic compounds and humic substances may have limited influence on microbial Hg methylation due to their complex structures and reduced bioavailability. While aromatic compounds and humic substances were not directly analyzed in this study, their complex structures likely reduce Hg bioavailability or slow microbial degradation, resulting in weaker effects on Hg methylation compared to low-molecular-weight organic acids. Future research could integrate direct Hg speciation measurements with detailed DOM compositional analyses to better understand how specific DOM components and Hg species interact to influence microbial Hg methylation.

DOM's influence on microbial Hg methylation has been observed in other ecosystems, such as wetlands and sediments, where DOM shapes microbial community structures to promote methylmercury (MeHg) production. For instance, in wetlands, DOM-bound Hg has been found to change the community assembly of mercury for methylating microbes (Fagervold et al., 2014). This highlights the broader ecological significance of DOM's role in promoting Hg methylation and suggest that DOM-driven microbiome modulation is a critical process across diverse environments. Moreover, the knowledge gained in this study highlights how variation in DOM quality due to human activities and climate change (e.g., changes in molecular weight, aromaticity, and bioactivity) could significantly alter MeHg production in different environmental compartments (Xenopoulos et al., 2021). For instance, long-term processes may scatter stable DOM, such as black carbon, globally through biomass combustion (Qi et al., 2020), while simpler and more reactive DOM may dominate in aquatic ecosystems (Xenopoulos et al., 2021). These changes could either enhance or diminish Hg ecotoxicity, depending on the specific conditions. Therefore, future in-depth studies coupling DOM quality, Hg speciation, and microbial Hg methylation are essential to deliver more accurate assessments of Hg's environmental and health impacts, particularly in the context of the Minamata Convention.

5 Conclusions

This study provides novel evidence that DOM significantly influences MeHg production by altering the composition and stimulating the activity of the core Hg-methylating microbiome. While DOM regulates the composition of other members of the Hg-methylating microbiome, its impact on MeHg production is primarily mediated through the core Hg-methylating microbiome. Using metagenomic binning and pure incubation experiments, we demonstrated that low-molecular-weight DOM directly promotes MeHg production by enhancing the metabolic activity of core Hg-methylating microorganisms. These findings underscore the central role of the core Hg-methylating microbiome in Hg cycling and highlight DOM as a critical driver of microbial Hg methylation. As human activities and climate change continue to alter DOM composition and concentration, their influence on Hg methylation dynamics warrants further investigation to better predict and mitigate Hg-related environmental and health risks.

Data Availability. The raw reads of *hgcA* gene amplicon sequencing have been deposited in the NCBI SRA under accession number PRJNA847325 and PRJNA972506. Shotgun metagenomic sequencing have been deposited in the

NCBI SRA under accession number PRJNA848068 and PRJNA972502. Other datasets generated during the current study are available from the corresponding author upon reasonable request.

Author Contributions. The study was designed by QP, BM, and XBF. QP, JL and YRL conducted the sampling, performed the DNA extraction and the bioinformatic analyses. JHH, KZ and MA performed the geochemical analyses. The manuscript was written by QP and BM, with assistance and input from co-authors.

Competing Interests. The contact author has declared that none of the authors has any competing interests.

Acknowledgments. We appreciate Prof. Alexandre J. Poulain (University of Ottawa, Canada) for his valuable advice on manuscript writing. We also appreciate Prof. Tao Jiang (Southwest University, China) for his important help in the analysis of natural organic matter. Our deep appreciation goes to Prof. Peng Liang (Zhejiang Agriculture and Forestry University) for generously providing *G. sulfurreducens* PCA. Additionally, we are grateful to Chen J., Kong K., Zhang Q.S. and Dr. Aslam M.W., for their help with sample collection and measurements.

Financial support. This work was financially supported by the National Natural Science Foundation of China (41931297 and 42207164) and Guizhou Provincial Science and Technology Projects (No. Qian-Ke-He-Ji-Chu ZK [2022] Yi-Ban 566).

376 **References**

377 Abdelhafiz, M. A., Liu, J., Jiang, T., Pu, Q., Aslam, M. W., Zhang, K., Meng, B., and Feng, X.: DOM influences Hg
378 methylation in paddy soils across a Hg contamination gradient, Environ. Pollut., 322, 121237,
379 https://doi.org/10.1016/j.envpol.2023.121237, 2023.
380 Archer E.: rfPermute: estimate permutation p-values for random forest importance metrics, https://CRAN.R-
381 project.org/package=rfPermute, 2018
382 Banerjee, S. K., Schlaeppi, K., and van der Heijden, M. G. A.: Keystone taxa as drivers of microbiome structure and
383 functioning, Nat. Rev. Microbiol., 16, 567-576, https://doi.org/10.1038/s41579-018-0024-1, 2018.
384 Barkay, T. and Gu, B.: Demethylation-The Other Side of the Mercury Methylation Coin: A Critical Review, ACS Environ.
385 Au, 2, 77-97, https://doi.org/10.1021/acsenvironau.1c00022, 2021.
386 Bastian, M., Heymann, S. and Jacomy, M.: Gephi: An Open Source Software for Exploring and Manipulating Networks,
387 In Proceedings of the Third International ICWSM Conference (pp. 361-362), https://gephi.org, 2009.
388 Blazejak, A., Erséus, C., Amann, R. and Dubilier, N.: Coexistence of bacterial sulfide oxidizers, sulfate reducers, and
389 spirochetes in a gutless worm (Oligochaeta) from the Peru margin, Appl. Environ. Microbiol., 71, 1553-1561, 2005.
390 Bravo, A. G., Zopfi, J., Buck, M., Xu, J., Bertilsson, S., Schaefer, J. K., Poté, J. W., and Cosio, C.: Geobacteraceae are
391 important members of mercury-methylating microbial communities of sediments impacted by waste water releases,
392 ISME J., 12, 802-812, https://doi.org/10.1038/s41396-017-0007-7, 2018.
393 Capo, E., Peterson, B. D., Kim, M., Jones, D. S., Acinas, S. G., Amyot, M., Bertilsson, S., Björn, E., Buck, M., Cosio, C.,
394 Elias, D. A., Gilmour, C. C., Goñi Urriza, M. S., Gu, B., Lin, H., Liu, Y., McMahon, K. D., Moreau, J. W., Pinhassi,
395 J., Podar, M., Puente-Sánchez, F., Sánchez, P., Storck, V., Tada, Y., Vigneron, A., Walsh, D. A., Vandewalle-Capo, M.,
396 Bravo, A. G., and Gionfriddo, C. M.: A consensus protocol for the recovery of mercury methylation genes from
397 metagenomes, Mol. Ecol. Resour., 23, 190-204, https://doi.org/10.1111/1755-0998.13687, 2022.
398 Chen, L., Jiang, Y., Liang, C., Luo, Y., Xu, Q., Han, C., Zhao, Q. G., and Sun, B.: Competitive interaction with keystone
399 taxa induced negative priming under biochar amendments, Microbiome, 7, https://doi.org/10.1186/s40168-019-0693-
400 7, 2019.
401 Chen, S., Zhou, Y., Chen, Y., and Gu, J.: fastp: an ultra-fast all-in-one FASTQ preprocessor, Bioinformatics, 34, i884-
402 i890, https://doi.org/10.1093/bioinformatics/bty560, 2018.
403 De Cáceres, M. and Legendre, P.: Associations between species and groups of sites: indices and statistical inference,
404 Ecology, 90, 3566-3574, https://doi.org/10.1890/08-1823.1, 2009.
405 Dong, W., Bian, Y., Liang, L., and Gu, B.: Binding constants of mercury and dissolved organic matter determined by a
406 modified ion exchange technique, Environ. Sci. Technol., 45, 3576-3583, https://doi.org/10.1021/es104207g, 2011.
407 Dray, S. and Dufour, A. B.: The ade4 Package: Implementing the Duality Diagram for Ecologists, J. Stat. Softw., 22, 1-
408 20, https://doi.org/10.18637/jss.v022.i04, 2007.
409 Driscoll, C. T., Mason, R. P., Chan, H. M., Jacob, D. J., and Pirrone, N.: Mercury as a Global Pollutant: Sources, Pathways,
410 and Effects, Environ. Sci. Technol., 47, 4967-4983, https://doi.org/10.1021/es305071v, 2013.
411 Eddy, S. R.: Accelerated Profile HMM Searches, Plos. Comput. Biol., 7, https://doi.org/10.1371/journal.pcbi.1002195,
412 2011.
413 Edgar, R. C.: UPARSE: highly accurate OTU sequences from microbial amplicon reads, Nat. Methods, 10, 996-998,
414 https://doi.org/10.1038/nmeth.2604, 2013.
415 Fagervold, S. K., Bourgeois, S., Pruski, A. M., Charles, F., Kerhervé, P., Vétion, G., and Galand, P. E.: River organic

matter shapes microbial communities in the sediment of the Rhône prodelta, ISME J., 8, 2327-2338, https://doi.org/10.1038/ismej.2014.86, 2014.

Feng, X., Li, P., Qiu, G., Wang, S. L., Li, G. H., Shang, L. H., Meng, B., jiang, H. W., Bai, W. Y., Li, Z. G., and Fu, X. W.: Human Exposure To Methylmercury through Rice Intake in Mercury Mining Areas, Guizhou Province, China, Environ. Sci. Technol., 42, 326-332, https://doi.org/10.1021/es071948x, 2008.

Finn, R. D., Clements, J., and Eddy, S. R.: HMMER web server: interactive sequence similarity searching, Nucleic Acids Res., 39, W29-W37, https://doi.org/10.1093/nar/gkr367, 2011.

Fortmann-Roe, S.: Consistent and Clear Reporting of Results from Diverse Modeling Techniques: The A3 Method, J. Stat. Softw., 66, 1-23, https://doi.org/10.18637/jss.v066.i07, 2015.

Frossard, A., Donhauser, J., Mestrot, A., Gygax, S., Bååth, E., and Frey, B.: Long- and short-term effects of mercury pollution on the soil microbiome, Soil. Biol. Biochem., 120, 191-199, https://doi.org/10.1016/j.soilbio.2018.01.028, 2018.

Fu, L., Niu, B., Zhu, Z., Wu, S., and Li, W.: CD-HIT: accelerated for clustering the next-generation sequencing data, Bioinformatics, 28, 3150-3152, https://doi.org/10.1093/bioinformatics/bts565, 2012.

Gilmour, C. C., Podar, M., Bullock, A. L., Graham, A. M., Brown, S. D., Somenahally, A. C., Johs, A., Hurt, R. A., Bailey, K. L., and Elias, D. A.: Mercury methylation by novel microorganisms from new environments, Environ. Sci. Technol., 47, 11810-11820, https://doi.org/10.1021/es403075t, 2013.

Gionfriddo, C., Capo, E., Peterson, B., Heyu, L., Jones, D., Bravo, A. G., Bertilsson, S., MOREAU, J., McMahon, K., Elias, D. and Gilmour, C.: Hg-MATEDb. v1.01142021 [Internet], https://smithsonian.figshare.com/articles/dataset/Hg-MATE Db_v1_01142021/13105370, 2021.

Gionfriddo, C. M., Wymore, A. M., Jones, D. S., Wilpiszeski, R. L., Lynes, M. M., Christensen, G. A., Soren, A., Gilmour, C. C., Podar, M. and Elias, D. A.: An Improved hgcAB Primer Set and Direct High-Throughput Sequencing Expand Hg-Methylator Diversity in Nature. Front Microbiol., 11, 541554, https://doi.org/10.3389/fmicb.2020.541554, 2020.

Graham, A. M., Aiken, G. R., and Gilmour, C. C.: Dissolved organic matter enhances microbial mercury methylation under sulfidic conditions, Environ. Sci. Technol., 46 5, 2715-2723, https://doi.org/10.1021/es203658f, 2012.

Helmrich, S., Vlassopoulos, D., Alpers, C. N., and O'Day, P. A.: Critical review of mercury methylation and methylmercury demethylation rate constants in aquatic sediments for biogeochemical modeling, Crit. Rev. Env. Sci. Tec., 52, 4353-4378, https://doi.org/10.1080/10643389.2021.2013073, 2021.

Hu, H., Umbreen, S., Zhang, Y., Bao, M., Huang, C., and Zhou, C.: Significant association between soil dissolved organic matter and soil microbial communities following vegetation restoration in the Loess Plateau, Ecol. Eng., 169, 106305, https://doi.org/10.1016/j.ecoleng.2021.106305, 2021.

Hu, H., Lin, H., Zheng, W., Tomanicek, S. J., Johs, A., Feng, X., Elias, D. A., Liang, L., and Gu, B.: Oxidation and methylation of dissolved elemental mercury by anaerobic bacteria, Nat. Geosci., 6, 751-754, https://doi.org/10.1038/ngeo1894, 2013.

Huerta-Cepas, J., Forslund, K., Coelho, L. P., Szklarczyk, D., Jensen, L. J., von Mering, C., and Bork, P.: Fast Genome-Wide Functional Annotation through Orthology Assignment by eggNOG-Mapper, Mol. Biol. Evol., 34, 2115-2122, https://doi.org/10.1093/molbev/msx148, 2016.

Hyatt, D., Chen, G. L., LoCascio, P. F., Land, M. L., Larimer, F. W., and Hauser, L. J.: Prodigal: Prokaryotic Gene Recognition and Translation Initiation Site Identification, BMC Bioinform., 11, 119, https://doi.org/10.1186/1471-2105-11-119, 2010.

Jiao, S., Qi, J., Jin, C., Liu, Y., Wang, Y., Pan, H., Chen, S., Liang, C., Peng, Z., Chen, B., Qian, X., and Wei, G.: Core phylotypes enhance the resistance of soil microbiome to environmental changes to maintain multifunctionality in

agricultural ecosystems, Global Change Biol., 28, 6653-6664, https://doi.org/10.1111/gcb.16387, 2022.

Jones, D. S., Walker, G. M., Johnson, N. W., Mitchell, C. P. J., Coleman Wasik, J. K., and Bailey, J. V.: Molecular evidence for novel mercury methylating microorganisms in sulfate-impacted lakes, ISME J., 13, 1659-1675, https://doi.org/10.1038/s41396-019-0376-1, 2019.

Joshi NA, Fass JN.: Sickle: A sliding-window, adaptive, quality-based trimming tool for FastQ files, https://github.com/najoshi/sickle, 2011.

Kassambara A. ggpubr.: 'ggplot2' based publication ready plots. R package version 0.2, https://CRAN.R-project.org/package=ggpubr, 2018.

Krogh, A., Larsson, B., Heijne, G. v., and Sonnhammer, E. L. L.: Predicting transmembrane protein topology with a hidden Markov model: application to complete genomes, J. Mol. Biol., 305 3, 567-580, https://doi.org/10.1006/jmbi.2000.4315, 2001.

Kujawinski, E. B.: The impact of microbial metabolism on marine dissolved organic matter, Annu. Rev. Mar., 3, 567-599, https://doi.org/10.1146/annurev-marine-120308-081003, 2011.

Li, D., Luo, R., Liu, C. M., Leung, C. M., Ting, H. F., Sadakane, K., Yamashita, H., and Lam, T. W.: MEGAHIT v1.0: A fast and scalable metagenome assembler driven by advanced methodologies and community practices, Methods, 102, 3-11, https://doi.org/10.1016/j.ymeth.2016.02.020, 2016.

Li, H., Wang, H., Wang, H. T., Xin, P. Y., Xu, X., Ma, Y., Liu, W. P., Teng, C. Y., Jiang, C., Lou, L. P., Arnold, W., Cralle, L., Zhu, Y. G., Chu, J. F., Gilbert, J. A., and Zhang, Z. J.: The chemodiversity of paddy soil dissolved organic matter correlates with microbial community at continental scales, Microbiome, 6, https://doi.org/10.1186/s40168-018-0561-x, 2018.

Li, Y. and Cai, Y.: Progress in the study of mercury methylation and demethylation in aquatic environments, Sci. Bull., 58, 177-185, https://doi.org/10.1007/s11434-012-5416-4, 2013.

Liaw, A. and Wiener, M. C.: Classification and Regression by randomForest, https://api.semanticscholar.org/CorpusID:3093707, 2002.

Liu, J., Chen, J., Poulain, A. J., Pu, Q., Hao, Z., Meng, B., and Feng, X.: Mercury and Sulfur Redox Cycling Affect Methylmercury Levels in Rice Paddy Soils across a Contamination Gradient, Environ. Sci. Technol., 57, 8149-8160, https://doi.org/10.1021/acs.est.3c02676, 2023.

Liu, J., Lu, B., Poulain, A. J., Zhang, R., Zhang, T., Feng, X., and Meng, B.: The underappreciated role of natural organic matter bond Hg(II) and nanoparticulate HgS as substrates for methylation in paddy soils across a Hg concentration gradient, Environ. Pollut., 292, 118321, https://doi.org/10.1016/j.envpol.2021.118321, 2022.

Liu, Y., Johs, A., Li, B., Lu, X., Hu, H., Sun, D. H., He, J. Z., and Gu, B.: Unraveling Microbial Communities Associated with Methylmercury Production in Paddy Soils, Environ. Sci. Technol., 52, 13110-13118, https://doi.org/10.1021/acs.est.8b03052, 2018.

Martin, M.: Cutadapt removes adapter sequences from high-throughput sequencing reads, EMBnet.journal, 17, 10-12, https://doi.org/10.14806/ej.17.1.200, 2011.

Meng, B., Feng, X., Qiu, G., Liang, P., Li, P., Chen, C., and Shang, L.: The process of methylmercury accumulation in rice (Oryza sativa L.), Environ. Sci. Technol., 45, 2711-2717, https://doi.org/10.1021/es103384v, 2011.

Muthayya, S., Sugimoto, J. D., Montgomery, S., and Maberly, G. F.: An overview of global rice production, supply, trade, and consumption, Annals of the New York Academy of Sciences, 1324, 7-14, https://doi.org/10.1111/nyas.12540, 2014.

Oksanen J, Blanchet F. G., Kindt R., Legendre P., Minchin P. R., O'Hara R. B., Simpson, G. L., Solymos, P., Steven, M. H. H. and Wagner, H.: Vegan: community ecology package. R package version 2.4-4, http://CRAN.R-

project.org/package=vegan, 2017.

Oloo, F. O., Valverde, A., Quiroga, M. V., Vikram, S., Cowan, D. A., and Mataloni, G.: Habitat heterogeneity and connectivity shape microbial communities in South American peatlands, Sci. Rep., 6, https://doi.org/10.1038/srep25712, 2016.

Oulhote, Y., Debes, F., Vestergaard, S., Weihe, P., and Grandjean, P.: Aerobic Fitness and Neurocognitive Function Scores in Young Faroese Adults and Potential Modification by Prenatal Methylmercury Exposure, Environ. Health Persp., 125, 677-683, https://doi.org/10.1289/EHP274, 2016.

Pankratov, T.A. and Dedysh, S.N.: Granulicella paludicola gen. nov., sp. nov., Granulicella pectinivorans sp. nov., Granulicella aggregans sp. nov. and Granulicella rosea sp. nov., acidophilic, polymer-degrading acidobacteria from Sphagnum peat bogs, Int J Syst Evol Microbiol, 60, 2951-2959, 2010.

Parks, D. H., Imelfort, M., Skennerton, C. T., Hugenholtz, P., and Tyson, G. W.: CheckM: assessing the quality of microbial genomes recovered from isolates, single cells, and metagenomes, Genome Res., 25, 1043-1055, https://doi.org/10.1101/gr.186072.114, 2015.

Parks, D. H., Chuvochina, M., Rinke, C., Mussig, A. J., Chaumeil, P. A., and Hugenholtz, P.: GTDB: an ongoing census of bacterial and archaeal diversity through a phylogenetically consistent, rank normalized and complete genome-based taxonomy, Nucleic Acids Res., 50, D785-D794, https://doi.org/10.1093/nar/gkab776, 2021.

Parks, J. M., Johs, A., Podar, M., Bridou, R., Hurt, R. A., Smith, S. D., Tomanicek, S. J., Qian, Y., Brown, S. D., Brandt, C. C., Palumbo, A. V., Smith, J. C., Wall, J. D., Elias, D. A., and Liang, L.: The Genetic Basis for Bacterial Mercury Methylation, Science, 339, 1332-1335, https://doi.org/10.1126/science.1230667, 2013.

Peterson, B. D., Krabbenhoft, D. P., McMahon, K. D., Ogorek, J. M., Tate, M. T., Orem, W. H., and Poulin, B. A.: Environmental formation of methylmercury is controlled by synergy of inorganic mercury bioavailability and microbial mercury-methylation capacity, Environ. Microbiol., https://doi.org/10.1111/1462-2920.16364, 2023.

Podar, M., Gilmour, C. C., Brandt, C., Soren, A. B., Brown, S. D., Crable, B. R., Palumbo, A., Somenahally, A., and Elias, D. A.: Global prevalence and distribution of genes and microorganisms involved in mercury methylation, Sci. Adv., 1, https://doi.org/10.1126/sciadv.1500675, 2015.

Qi, Y., Fu, W., Tian, J., Luo, C., Shan, S., Sun, S., Ren, P., Zhang, H., Liu, J., Zhang, X., and Wang, X.: Dissolved black carbon is not likely a significant refractory organic carbon pool in rivers and oceans, Nat. Commun., 11, https://doi.org/10.1038/s41467-020-18808-8, 2020.

Revelle, W.: psych: Procedures for Psychological, Psychometric, and Personality Research, Northwestern University, Evanston, Illinois, USA, https://CRAN.R-project.org/package=psych, 2023.

Roman, H. A., Walsh, T. L., Coull, B., Dewailly, É., Guallar, E., Hattis, D. B., Mariën, K., Schwartz, J. D., Stern, A. H., Virtanen, J. K., and Rice, G. E.: Evaluation of the Cardiovascular Effects of Methylmercury Exposures: Current Evidence Supports Development of a Dose–Response Function for Regulatory Benefits Analysis, Environ. Health Persp., 119, 607 - 614, https://doi.org/10.1289/ehp.1003012, 2011.

Sakai, S., Conrad, R., Liesack, W., and Imachi, H.: Methanocella arvoryzae sp. nov., a hydrogenotrophic methanogen isolated from rice field soil, Int. J. Syst. Evol. Micr., 60, 2918-2923, https://doi.org/10.1099/ijs.0.020883-0, 2010.

Schartup, A. T., Ndu, U., Balcom, P. H., Mason, R. P., and Sunderland, E. M.: Contrasting effects of marine and terrestrially derived dissolved organic matter on mercury speciation and bioavailability in seawater, Environ. Sci. Technol., 49, 5965-5972, https://doi.org/10.1021/es506274x, 2015.

Schartup, A. T., Thackray, C. P., Qureshi, A., Dassuncao, C., Gillespie, K. M., Hanke, A. R., and Sunderland, E. M.: Climate change and overfishing increase neurotoxicant in marine predators, Nature, 572, 648-650, https://doi.org/10.1038/s41586-019-1468-9, 2019.

Schöne, C., Poehlein, A., Jehmlich, N., Adlung, N., Daniel, R., von Bergen, M., Scheller, S., and Rother, M.: Deconstructing Methanosarcina acetivorans into an acetogenic archaeon, Proc. Natl. Acad. Sci. USA., 119, https://doi.org/10.1073/pnas.2113853119, 2022.

Skyllberg, U., Bloom, P. R., Qian, J., Lin, C.-M., and Bleam, W. F.: Complexation of mercury(II) in soil organic matter: EXAFS evidence for linear two-coordination with reduced sulfur groups, Environ. Sci. Technol., 40, https://doi.org/4174-4180, 10.1021/es0600577, 2006.

Sunagawa, S., Coelho, L. P., Chaffron, S., Kultima, J. R., Labadie, K., Salazar, G., Djahanschiri, B., Zeller, G., Mende, D. R., Alberti, A., Cornejo-Castillo, F. M., Costea, P. I., Cruaud, C., d'Ovidio, F., Engelen, S., Ferrera, I., Gasol, J. M., Guidi, L., Hildebrand, F., Kokoszka, F., Lepoivre, C., Lima-Mendez, G., Poulain, J., Poulos, B. T., Royo-Llonch, M., Sarmento, H., Vieira-Silva, S., Dimier, C., Picheral, M., Searson, S., Kandels-Lewis, S., Bowler, C., Vargas, C. d., Gorsky, G., Grimsley, N. H., Hingamp, P., Iudicone, D., Jaillon, O., Not, F., Ogata, H., Pesant, S., Speich, S., Stemmann, L., Sullivan, M. B., Weissenbach, J., Wincker, P., Karsenti, E., Raes, J., Acinas, S. G., and Bork, P.: Structure and function of the global ocean microbiome, Science, 348, https://doi.org/10.1126/science.1261359, 2015.

Tao, S., Fang, J., Zhao, X., Zhao, S., Shen, H., Hu, H., Tang, Z., Wang, Z., and Guo, Q.: Rapid loss of lakes on the Mongolian Plateau, Proc. Natl. Acad. Sci. USA., 112, 2281-2286, https://doi.org/10.1073/pnas.1411748112, 2015.

Ullrich, S. M., Tanton, T. W., and Abdrashitova, S. A.: Mercury in the Aquatic Environment: A Review of Factors Affecting Methylation, Crit. Rev. Env. Sci. Tec., 31, 241-293, https://doi.org/10.1080/20016491089226, 2001.

Uritskiy, G., DiRuggiero, J., and Taylor, J.: MetaWRAP—a flexible pipeline for genome-resolved metagenomic data analysis, Microbiome, 6, https://doi.org/10.1186/s40168-018-0541-1, 2018.

Wang, L., Wang, L.-a., Zhan, X., Huang, Y., Wang, J., and Wang, X.: Response mechanism of microbial community to the environmental stress caused by the different mercury concentration in soils, Ecotox. Environ. Safe., 109906, https://doi.org/10.1016/j.ecoenv.2019.109906, 2019.

Wickham, H. (eds): ggplot2 - Elegant Graphics for Data Analysis, Springer-Verlag, New York, https://doi.org/10.1007/978-0-387-98141-3, 2009.

Xenopoulos, M. A., Barnes, R. T., Boodoo, K. S., Butman, D. E., Catalán, N., D'Amario, S. C., Fasching, C., Kothawala, D., Pisani, O., Solomon, C. T., Spencer, R. G. M., Williams, C. J., and Wilson, H. F.: How humans alter dissolved organic matter composition in freshwater: relevance for the Earth's biogeochemistry, Biogeochemistry, 154, 323-348, https://doi.org/10.1007/s10533-021-00753-3, 2021.

Xun, W., Liu, Y., Li, W., Ren, Y., Xiong, W., Xu, Z., Zhang, N., Miao, Y., Shen, Q., and Zhang, R.: Specialized metabolic functions of keystone taxa sustain soil microbiome stability, Microbiome, 9, https://doi.org/10.1186/s40168-020-00985-9, 2021.

Yin, Y., Li, Y., Ma, X., Liu, J. and Jiang, G.: Role of Natural Organic Matter in the Biogeochemical Cycle of Mercury : Binding and Molecular Transformation, Prog. Chem., 25, 2169-2177, https://doi.org/10.1016/j.scitotenv.2021.152047, 2013

Zhang, H., Feng, X., Larssen, T., Qiu, G. and Vogt, R. D.: In inland China, rice, rather than fish, is the major pathway for methylmercury exposure, Environ. Health Persp., 118, 1183-1188, 2010.

Zhang, R., Aris-Brosou, S., Storck, V., Liu, J., Abdelhafiz, M. A., Feng, X., Meng, B., and Poulain, A. J.: Mining-impacted rice paddies select for Archaeal methylators and reveal a putative (Archaeal) regulator of mercury methylation, ISME Commun., 3, https://doi.org/10.1038/s43705-023-00277-x, 2023.

Zhao, L., Chen, H., Lu, X., Lin, H., Christensen, G. A., Pierce, E. M., and Gu, B.: Contrasting Effects of Dissolved Organic Matter on Mercury Methylation by Geobacter sulfurreducens PCA and Desulfovibrio desulfuricans ND132, Environ. Sci. Technol., 51 18, 10468-10475, https://doi.org/10.1021/acs.est.7b02518, 2017.

584 Zhong, H., Tang, W., Li, Z., Sonne, C., Lam, S. S., Zhang, X., Kwon, S. Y., Rinklebe, J., Nunes, L. M., Yu, R. Q., Gu, B.,
585 Hintelmann, H., Tsui, M. T. K., Zhao, J., Zhou, X. Q., Wu, M., Liu, B., Hao, Y., Chen, L., Zhang, B., Tan, W., Zhang,
586 X. X., Ren, H. and Liu, Y. R.: Soil Geobacteraceae are the key predictors of neurotoxic methylmercury
587 bioaccumulation in rice, Nature Food, 5, 301-311, 2024.
588

Supplement of

Dissolved organic matter fosters core mercury-methylating microbiome for methylmercury production in paddy soils

Qiang Pu et al.

Correspondence to: Bo Meng (mengbo@mail.gyig.ac.cn)

Supplementary Texts

Text S1. Measurement of soil physico-chemical properties, mercury and dissolved organic matter.

S1.1 Characterization of soil physico-chemical properties.

Soil pH was measured using a pH meter (PD-501, SANXIN, China) after extracting 10 g of soil with ultrapure deionized water (soil: water = 1:2.5 w/v). Soil total carbon and total nitrogen were measured by an organic elemental analyzer (vario MACRO cube, Elementar, Germany) using 0.05 g of soil samples. Water-soluble SO_4^{2-} was extracted from 1 g of soil with ultrapure deionized water in a 1:10 w/v ratio using a horizontal oscillator at 220 rpm for 16 h in the dark. The supernatant solution was obtained by centrifugation (2500 × g for 10 min) and filtration (0.45 μm, PES, Bizcomr, China). Water-soluble SO_4^{2-} was analyzed with a UV-Vis spectrophotometer (UV-5100B, METASH, China). Water-soluble NO_3^- was extracted from 1 g of soil with 50 mL of 2 M KCl, then filtered using PES membranes (0.45 μm, Bizcomr, China), and measured by UV spectrophotometry (UV-1200, Macy Analysis Instrument Co. Ltd., China). The S^{2-} and Fe^{2+} in soil pore water were obtained by centrifuging fresh soil samples in 50 mL centrifuge tubes at 3500 × g for 15 minutes. The S^{2-} in soil pore water was measured by using methylene blue method (Cline, 1969), with a detection limit of 0.13 μM. The Fe^{2+} in soil pore water was measured by using ferrozine method (Viollier et al., 2000), with a detection of 10 μM.

S1.2 Analysis of mercury.

The water-soluble Hg (representing Hg bioavailability) in paddy soils was extracted according to Shi et al. with slight modifications (Shi et al., 2005). Briefly, ~0.5 g of soil was extracted in 8 mL of Milli-Q water with continuous agitation for 2 h. The suspension was centrifuged at 2850 g for 30 min and vacuum filtered through 0.45-μm mixed cellulose acetate filters (Whatman, USA). The amount of water-soluble Hg in solution was measured by cold vapor atomic fluorescence spectrometry (CVAFS, Brooks Rand Model III, Brooks Rand Laboratories) according to USEPA method 1631 (EPA, 2002). To determine total Hg (THg), ~0.2 g of soil was digested in 5 mL of freshly prepared aqua regia ($HCl:HNO_3$ = 3:1 v/v) with 5 mL of Milli-Q water at 95 ℃ for 55 mins. The total Hg amount in the digest solution was measured by cold vapor atomic fluorescence spectrometry (CVAFS, Brooks Rand Model III, Brooks Rand Laboratories) according to USEPA method 1631 (EPA, 2002). Approximately 0.3-0.4 g of soil was

extracted using $CuSO_4$-methanol solvent for MeHg quantification via gas chromatography CVAFS (GC-CVAFS, Brooks Rand Model III, Brooks Rand Laboratories) following the procedure of USEPA method 1630 (EPA, 2001). To ensure the accuracy of THg and MeHg quantification in soils, method blanks and standard reference materials, GSS-5 (THg: 290 ± 30 ng g^{-1}) and ERMCC580 (MeHg: 75.5 ± 3.7 ng g^{-1}), were analyzed. The THg and MeHg recoveries from GSS-5 and ERMCC580 were 113.0% ± 7.1% (n=6) and 103.6% ± 3.5% (n = 3), respectively. The relative standard deviation (RSD%) for THg and MeHg analysis in triplicate was less than 5.2% and 3.9%, respectively.

S1.3 Analysis of dissolved organic matter concentration and composition.

The concentration of soil dissolved organic matter (DOM), reflected by water-soluble dissolved organic carbon, was determined by extracting 1 g of soil with Milli-Q water in a 1:10 w/v ratio. The extract was then filtered using 0.45 μm polypropylene membrane filters and analyzed using a total organic carbon analyzer (Vario TOC cube, Elementar, Germany). The dissolved organic matter composition (reflected by optical properties of DOM) was characterized with UV-Vis absorption through Aqualog® absorption-fluorescence spectroscopy (Jobin Yvon, Horiba, Japan) on the same extract used for measuring DOC concentration. UV-Vis absorption spectra for liquid samples were scanned from 230 nm to 800 nm (1 nm interval) (Liu et al., 2022). Internal filtering effects were minimized via pre-measurement dilution to a DOC < 10 mg/L (Jiang et al., 2018). S_R (spectral slope ratio over the ranges of 275-295 nm and 350-400 nm) of DOM was calculated for the optical property of DOM, and the detailed calculation and description can be found in previous works (Jiang et al., 2018; Zhang et al., 2023).

S1.4 Analysis of low-molecular-weight organic acids.

Soils from NMS, MMS and HMS were selected for analysis of low-molecular-weight organic acids. Soil (~10 g) was extracted with 20 mL milli-Q water for 12 h. The mixture was centrifuged at 15 000 × g for 15 min, and filtered through Whatman No. 42. Water-soluble low-molecular-weight organic acids were obtained by evaporating the solvent to dryness in a rotary evaporator at 40 °C and redissolving the residue in 1 mL of Mill-Q water. The water-soluble low-molecular-weight organic acids were identified and quantified by using reversed-phase high-performance liquid chromatography (HPLC, Shimadzu LC-20, Shimadzu, Osaka, Japan) with a diode array detector (van Hees et al., 1999).

Text S2. *hgcA* gene quantification.

The abundance of the *hgcA* gene was quantified with primer set ORNL-Delta-HgcA-F: GCCAACTACAAGMTGASCTWC and ORNL-Delta-HgcA-R: CCSGCNGCRCACCAGACRTT in AB 7500 (Applied Biosystems, USA). The PCR setup was as follows: 10 µl of SYBR Premix Ex Taq (TaKaRa Bio Inc., Japan), 0.5 µL (10 mM) of each primer, 2 µL of diluted DNA template (~20 ng), and 7 µL of sterilized DDW (double distilled water). The *hgcA* gene was quantified in triplicate under the following thermal cycles: 3 min initial denaturation at 95°C, 40 cycles of 15 s at 95°C, 15 s at 50°C, and 15 s at 55°C, and 4 min at 72°C, followed by a plate read at 83 °C (Liu et al., 2018). Three no-template controls were used to detect contamination during the amplification process.

Text S3. Bacterial culture and validation experiment.

Geobacter sulfurreducens PCA was cultured in nutrient broth (NB) at 33°C (Hu et al., 2013). Cells were harvested at the middle log phase and washed three times with phosphate buffered saline (PBS, containing 0.137 M sodium chloride, 0.0027 M potassium chloride, 0.01 M sodium phosphate dibasic, and 0.0018 M potassium phosphate monobasic, pH 7.4) media before the validation experiment.

The natural DOM solution was extracted from paddy soils from the second sampling campaign. First, we divided the 19 paddy soil samples into NMS, MMS, and HMS based on mercury concentrations (see Table S1 for the classification results). Then, we mixed all paddy soil samples within each group (NMS, MMS, and HMS) in equal proportions to obtain homogenized samples for each group. Next, we extracted the dissolved organic matter from the soil using a soil-to-water ratio of 1:10 (w/v). The extracted solution was then split into two portions: one for the determination of organic matter composition and the other for validation experiments.

Serum bottles (100 mL, borosilicate glass bottle; BKMAM Biotechnology, China) were used for the validation experiment in an oxygen-free glovebox (PLASLABS, USA). The experiment was conducted in PBS medium, supplemented with 5 mL of natural DOM solution extracted from paddy soils (i.e., NMS, MMS and HMS), $HgCl_2$ (1.36 μg/L; Sinopharm Chemical Reagent Co., Ltd., China), and a cell density of 2×10^8 cells mL^{-1}. All vials were immediately sealed with caps and kept in the dark on shaker. After incubation for 24 h at 33°C, triplicate sample vials were remove from the shaker and preserved at 4°C. An aliquot (10 mL) was filtered through 0.45 μm polyethersulfone (PES) membranes and analyzed for DOM concentration via total organic carbon analyzer (Vario TOC cube, Elementar, Germany). Another aliquot of the sample (3 mL) was acidified with trace metal grade HCl (0.2% (v/v)) and acetic acid (0.5% (v/v)), and analyzed for MeHg. The remaining aliquot was oxidized overnight in BrCl (1% (v/v)) and analyzed for total Hg. Total Hg and MeHg were measured by CVAFS (Brooks Rand Model III, Brooks Rand Laboratories) and cold vapor atomic fluorescence spectrometry (CVAFS, Brooks Rand Model III, Brooks Rand Laboratories), respectively (EPA, 2001; 2002).

To monitor abiotic Hg methylation, the aforementioned experiment was conducted as described above, without addition of bacterial cells.

Supplementary Figures

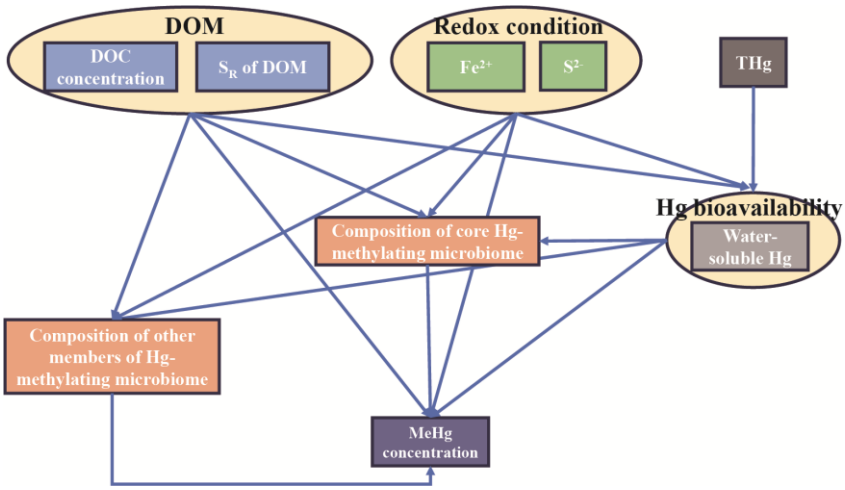

Fig. S1. A *priori* models for the structure equation models of variation in MeHg production based on the hypothesized causal relationships between multiple factors and MeHg production.

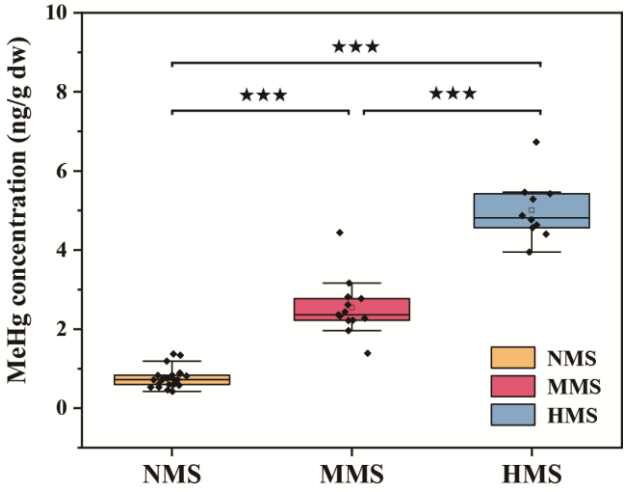

Fig. S2. Soil MeHg concentration in paddy soils. NMS, non-Hg polluted paddy soils (n = 23); MMS, moderate Hg-polluted paddy soils (n = 13); HMS, high Hg-polluted paddy soils (n = 10). "★★★" represents significant difference between different paddy soils ($p < 0.001$).

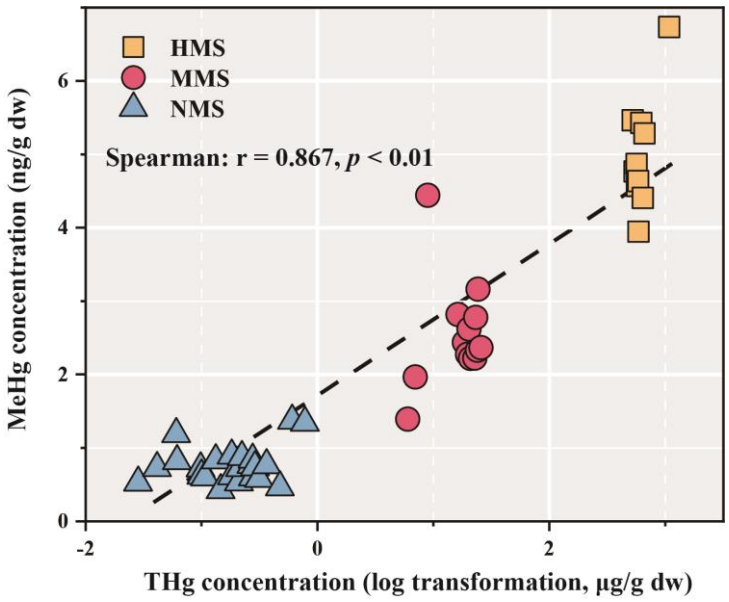

Fig. S3. Correlation between THg and MeHg concentration in paddy soils. NMS, non-Hg polluted paddy soils (n = 23); MMS, moderate Hg-polluted paddy soils (n = 13); HMS, high Hg-polluted paddy soils (n = 10).

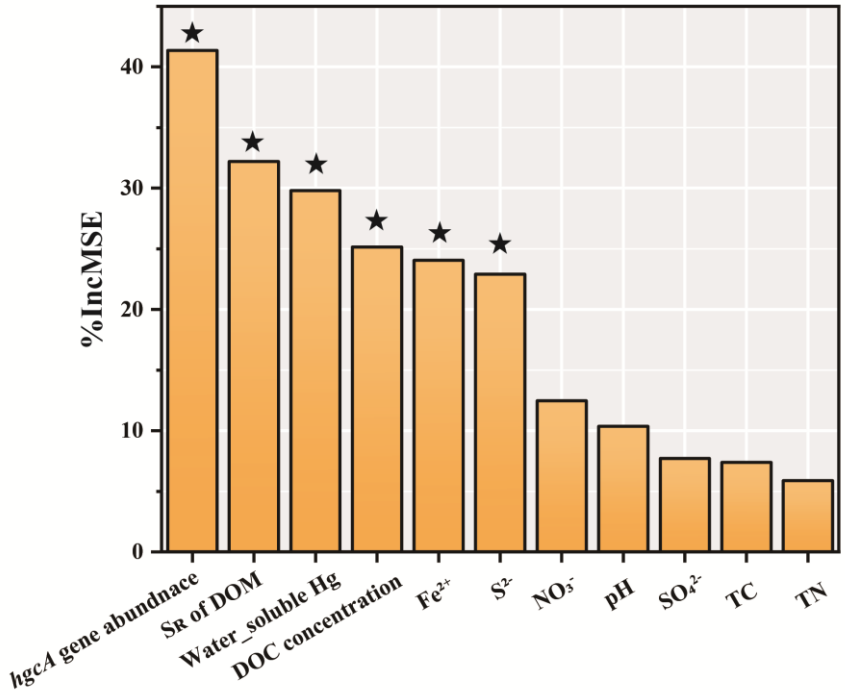

Fig. S4. Random forest modeling indicating the importance of different predictors for MeHg production. The number of trees used in model is 5000. "★" represents a statistically significant predictor ($p < 0.05$).

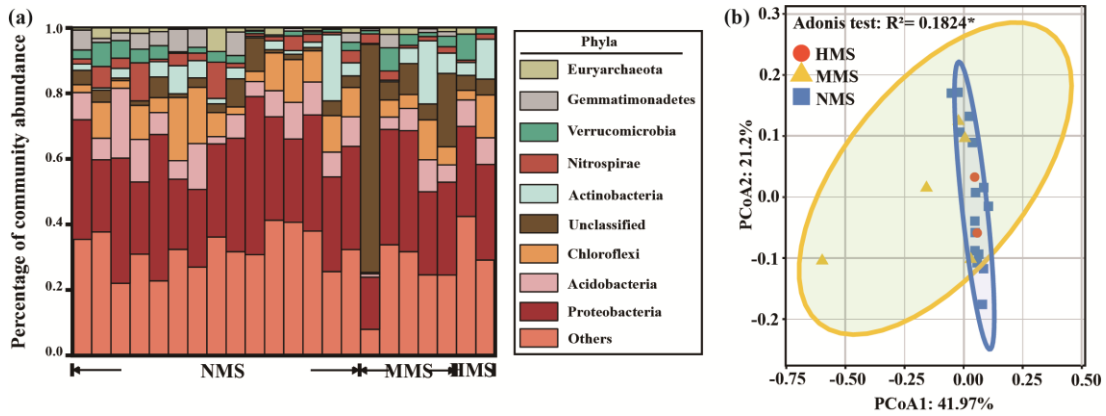

Fig. S5. (a) Hg-methylating microbial community composition in different paddy soils based on metagenomic sequencing. Phyla with low abundance phyla grouped together under "other phyla". **(b)** Principal coordinates analysis (PCoA) based on Bray-curtis distance showing the overall pattern of Hg-methylating microbial communities in paddy soils. NMS, non-Hg polluted paddy soils (n = 15); MMS, moderate Hg-polluted paddy soils (n = 5); HMS, high Hg-polluted paddy soils (n = 2).

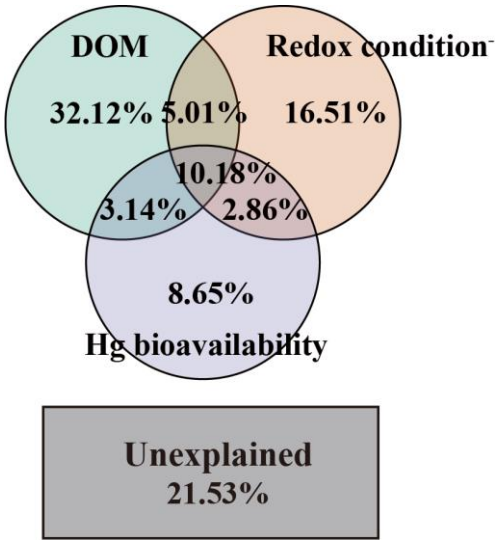

Fig. S6. Variation partitioning analysis differentiating effects of DOM, redox conditions, and Hg bioavailability on core Hg-methylating microbiome composition. DOM is reflected by DOM concentration and composition, which are measured as water-soluble DOC concentration and S_R (spectral slope ratio of $S_{275-295}$:$S_{350-400}$) values of DOM. Redox conditions are reflected by soil Fe^{2+} and S^{2-}, which are measured as concentrations of Fe^{2+} and S^{2-} in soil pore water. Hg bioavailability is reflected by water-soluble Hg. It should be noted that Fe^{2+} and S^{2-} data were limited to the soil samples obtained in August 2022.

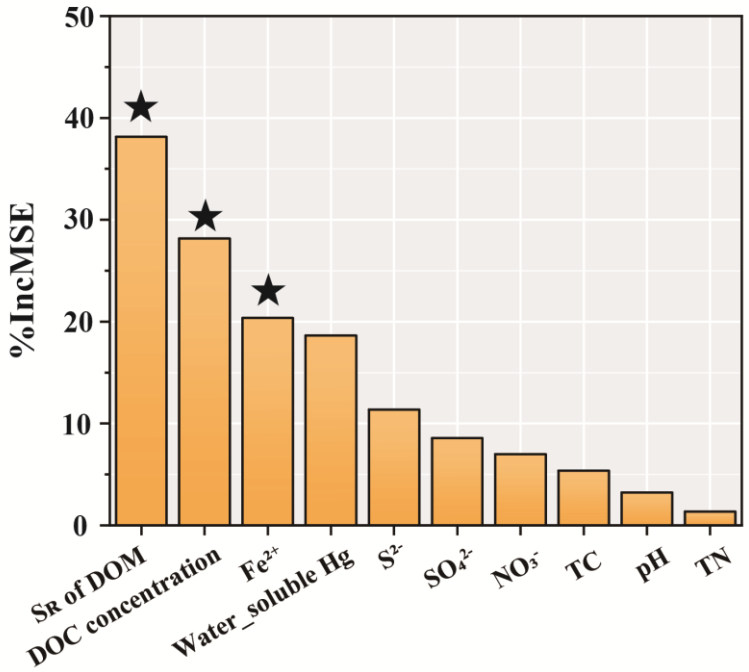

Fig. S7. Random forest modeling indicating the importance of different predictors for core Hg-methylating microbiome composition. The number of trees used in model is 5000. "★" represents a statistically significant predictor ($p < 0.05$).

Supplementary Tables

Table S1. Detailed information for paddy soils collected from 12 provinces across China.

Sample	Province	Site	Longitude	Latitude	Total Hg (μg/g)	Sampling time	Category
S1	Guizhou	HX-1	106°31′34″	26°25′15″	0.22	Sep. 2020	NMS
S2	Guizhou	HX-2	106°31′20″	26°25′18″	0.27	Sep. 2020	NMS
S3	Guizhou	HX-3	106°31′21″	26°25′15″	0.29	Sep. 2020	NMS
S4	Guizhou	HX-4	106°31′28″	26°25′16″	0.31	Sep. 2020	NMS
S5	Guizhou	HX-5	106°31′19″	26°25′17″	0.28	Sep. 2020	NMS
S6	Guizhou	HX-6	106°31′26″	26°25′21″	0.28	Sep. 2020	NMS
S7	Guizhou	HX-7	106°31′31″	26°25′20″	0.36	Sep. 2020	NMS
S8	Guizhou	HX-8	106°31′28″	26°25′14″	0.18	Sep. 2020	NMS
S9	Guizhou	HX-9	106°31′15″	26°25′19″	0.21	Sep. 2020	NMS
S10	Guizhou	GX-1	109°09′25″	27°33′23″	19.74	Sep. 2020	MMS
S11	Guizhou	GX-2	109°11′22″	27°33′37″	24.3	Sep. 2020	MMS
S12	Guizhou	GX-3	109°10′09″	27°33′36″	20.24	Sep. 2020	MMS
S13	Guizhou	GX-4	109°12′42″	27°33′53″	23.94	Sep. 2020	MMS
S14	Guizhou	GX-5	109°11′02″	27°33′28″	22.79	Sep. 2020	MMS
S15	Guizhou	GX-6	109°13′38″	27°33′56″	25.67	Sep. 2020	MMS
S16	Guizhou	GX-7	109°10′35″	27°33′33″	23.25	Sep. 2020	MMS
S17	Guizhou	GX-8	109°09′55″	27°33′43″	20.86	Sep. 2020	MMS
S18	Guizhou	GX-9	109°09′12″	27°33′31″	18.56	Sep. 2020	MMS
S19	Guizhou	SK-1	109°12′34″	27°30′41″	639.87	Sep. 2020	HMS
S20	Guizhou	SK-2	109°12′48″	27°31′05″	586.56	Sep. 2020	HMS
S21	Guizhou	SK-3	109°12′24″	27°30′36″	524.16	Sep. 2020	HMS
S22	Guizhou	SK-4	109°12′27″	27°30′25″	543.04	Sep. 2020	HMS
S23	Guizhou	SK-5	109°12′35″	27°30′39″	583.72	Sep. 2020	HMS
S24	Guizhou	SK-6	109°12′18″	27°30′50″	567.14	Sep. 2020	HMS
S25	Guizhou	SK-7	109°12′30″	27°30′52″	621.2	Sep. 2020	HMS
S26	Guizhou	SK-8	109°12′38″	27°30′55″	570.8	Sep. 2020	HMS
S27	Guizhou	SK-9	109°12′49″	27°31′02″	661.62	Sep. 2020	HMS
S28	Jilin	5N-3	125°57′0″	43°42′54″	0.03	Aut. 2022	NMS
S29	Jilin	5N-8	125°44′7″	44°6′26″	0.06	Aut. 2022	NMS
S30	Liaoning	5M-5	123°6′45″	41°49′46″	0.04	Aut. 2022	NMS
S31	Hubei	3I-1	113°10′48″	29°31′48″	0.06	Aut. 2022	NMS
S32	Guangxi	1A-28	108°45′58″	21°48′23″	0.1	Aut. 2022	NMS
S33	Hunan	3I-11	112°24′0″	28°34′12″	0.1	Aut. 2022	NMS
S34	Guangdong	1B-14	110°43′25″	21°51′23″	0.11	Aut. 2022	NMS
S35	Guangxi	1A-22	110°14′59″	22°21′20″	0.13	Aut. 2022	NMS
S36	Sichuan	3K-3	104°20′24″	30°49′12″	0.15	Aut. 2022	NMS
S37	Guizhou	4G-15	106°20′28″	26°25′59″	0.18	Aut. 2022	NMS
S38	Jiangsu	2E-11	119°9′29″	33°28′45″	0.21	Aut. 2022	NMS
S39	Hunan	3I-18	109°38′24″	28°37′12″	0.48	Aut. 2022	NMS
S40	Guangxi	1A-1	109°45′33″	23°11′26″	0.61	Aut. 2022	NMS
S41	Zhejiang	2D-5	119°41′31″	30°19′6″	0.78	Aut. 2022	NMS
S42	Liaoning	5M-1	123°7′9″	41°19′15″	6.01	Aut. 2022	MMS
S43	Shaannxi	6Q-23	109°27′55″	33°5′1″	7	Aut. 2022	MMS
S44	Guizhou	4G-8	109°24′38″	27°39′59″	8.95	Aut. 2022	MMS
S45	Guizhou	4G-7	109°15′13″	27°31′58″	16.34	Aut. 2022	MMS
S46	Chongqin	3J-1	108°55′12″	28°37′48″	1079.75	Aut. 2022	HMS

Paddy soils were divided into three categories according to mercury concentration: NMS, non-Hg polluted soils; MMS, moderate Hg-polluted soils; HMS, high Hg-polluted soils. Aut., August; Sep., September.

Table S2. Characterization of dissolved organic matter (DOM) in paddy soils.

Sample	Category	Site	DOM concentration ($g\ kg^{-1}$)	DOM composition [a]				
				$SUVA_{254}$	S_R	BIX	FI	HIX
S1	NMS	HX-1	0.36	1.21	1.9	0.63	1.48	0.8
S2	NMS	HX-2	0.36	0.65	0.54	0.69	1.57	0.7
S3	NMS	HX-3	0.37	0.85	1	0.66	1.57	0.73
S4	NMS	HX-4	0.43	1.27	1.28	0.6	1.48	0.78
S5	NMS	HX-5	0.38	0.6	1.2	0.7	1.57	0.71
S6	NMS	HX-6	0.38	1.5	0.99	0.61	1.47	0.83
S7	NMS	HX-7	0.43	0.81	1.2	0.64	1.53	0.76
S8	NMS	HX-8	0.36	0.6	0.51	0.7	1.57	0.71
S9	NMS	HX-9	0.34	1.32	1.7	0.66	1.53	0.76
S10	MMS	GX-1	0.36	1.12	0.77	0.51	1.55	0.99
S11	MMS	GX-2	0.36	0.97	0.82	0.52	1.54	0.98
S12	MMS	GX-3	0.36	0.09	0.79	0.5	1.37	0.88
S13	MMS	GX-4	0.39	1.14	0.93	0.52	1.4	0.98
S14	MMS	GX-5	0.38	1.03	0.92	0.5	1.42	1
S15	MMS	GX-6	0.38	1.01	0.97	0.6	1.59	0.93
S16	MMS	GX-7	0.37	0.63	0.84	0.58	1.5	0.85
S17	MMS	GX-8	0.37	1.08	0.82	0.54	1.42	0.87
S18	MMS	GX-9	0.38	1.14	0.89	0.58	1.5	0.77
S19	HMS	SK-1	0.21	1.04	0.42	0.51	1.17	0.75
S20	HMS	SK-2	0.2	1.08	0.39	0.52	1.19	0.72
S21	HMS	SK-3	0.32	1.32	0.57	0.44	1.08	0.77
S22	HMS	SK-4	0.19	1.53	0.39	0.62	1.24	0.56
S23	HMS	SK-5	0.33	1.15	0.6	0.45	1.2	0.78
S24	HMS	SK-6	0.31	1.48	0.35	0.45	1.12	0.7
S25	HMS	SK-7	0.28	1.59	0.56	0.42	1.06	0.77
S26	HMS	SK-8	0.32	1.16	0.35	0.53	1.2	0.74
S27	HMS	SK-9	0.27	1.15	0.49	0.45	1.2	0.78
S28	NMS	5N-3	0.61	0.16	1.2	0.76	1.63	0.95
S29	NMS	5N-8	0.56	0.12	4.1	0.76	1.57	1
S30	NMS	5M-5	0.54	0.33	1.21	0.94	1.69	0.91
S31	NMS	3I-1	0.5	0.31	1.13	0.63	1.63	0.84
S32	NMS	1A-28	0.64	1.11	0.86	0.57	1.47	0.93
S33	NMS	3I-11	0.51	0.23	1.21	0.65	1.64	0.9
S34	NMS	1B-14	0.55	0.18	1.72	0.57	1.77	0.86
S35	NMS	1A-22	0.51	0.22	2.87	0.83	1.66	0.79
S36	NMS	3K-3	0.58	0.74	1.34	0.54	1.5	0.89
S37	NMS	4G-15	0.33	0.38	1.47	0.56	1.56	0.95
S38	NMS	2E-11	0.5	0.68	1.2	0.5	1.46	0.98
S39	NMS	3I-18	0.45	0.29	0.91	0.55	1.64	0.9
S40	NMS	1A-1	0.89	0.17	1.13	0.73	1.75	0.87
S41	NMS	2D-5	0.54	1.53	1.32	0.73	1.97	0.34
S42	MMS	5M-1	0.39	0.32	0.84	0.58	1.44	0.98
S43	MMS	6Q-23	0.42	0.39	1.06	0.54	1.57	0.92
S44	MMS	4G-8	0.4	0.41	0.99	0.68	1.64	0.79
S45	MMS	4G-7	0.61	0.64	0.93	0.76	1.63	0.95
S46	HMS	3J-1	0.53	1.75	0.52	0.55	1.14	0.62

Paddy soils were divided into three categories according to mercury concentration: NMS, non-Hg polluted soils; MMS, moderate Hg-polluted soils; HMS, high Hg-polluted soils.

[a] $SUVA_{254}$ (specific UV absorbance at a wavelength of 254 nm) and S_R (spectral slope ratio of $S_{275\text{-}295}$: $S_{350\text{-}400}$) are properties from UV-Vis absorption spectra of DOM.

biological index (BIX), humification index (HIX) and fluorescence index (FI) are the fluorescence compounds and calculated indices from EEM fluorescence spectra of DOC.

Table S3. Physicochemical properties in paddy soils

Sample	Category	Site	pH	SO_4^{2-} (mg kg^{-1})	NO_3^- (mg kg^{-1})	TN (%)	TC (%)	S^{2-} (μM)	Fe^{2+} (μM)
S1	NMS	HX-1	7.52	347.87	17.67	0.4	5.49	No data	No data
S2	NMS	HX-2	7.53	369.9	19.52	0.28	3.15	No data	No data
S3	NMS	HX-3	7.51	354.61	18.38	0.41	5.47	No data	No data
S4	NMS	HX-4	7.5	369.68	20.26	0.41	5.5	No data	No data
S5	NMS	HX-5	7.52	356.8	18.73	0.21	7.82	No data	No data
S6	NMS	HX-6	7.54	351.22	18.24	0.29	3.13	No data	No data
S7	NMS	HX-7	7.51	358.16	18.76	0.21	7.79	No data	No data
S8	NMS	HX-8	7.53	343.73	18.26	0.29	3.15	No data	No data
S9	NMS	HX-9	7.51	348.69	18.21	0.21	7.77	No data	No data
S10	MMS	GX-1	7.52	348.01	17.62	0.42	5.72	No data	No data
S11	MMS	GX-2	7.52	349.67	17.55	0.21	7.99	No data	No data
S12	MMS	GX-3	7.5	337.66	17.57	0.42	5.74	No data	No data
S13	MMS	GX-4	7.5	371.17	17.78	0.28	3.21	No data	No data
S14	MMS	GX-5	7.49	335.06	17.63	0.43	5.71	No data	No data
S15	MMS	GX-6	7.5	381.51	17.79	0.27	3.19	No data	No data
S16	MMS	GX-7	7.5	333.01	17.6	0.47	6.08	No data	No data
S17	MMS	GX-8	7.51	377.65	17.55	0.21	7.88	No data	No data
S18	MMS	GX-9	7.5	339.97	17.5	0.21	7.93	No data	No data
S19	HMS	SK-1	7.51	254.52	15.65	0.48	6.12	No data	No data
S20	HMS	SK-2	7.48	255.55	14.58	0.21	7.84	No data	No data
S21	HMS	SK-3	7.47	266.23	16.1	0.46	6.1	No data	No data
S22	HMS	SK-4	7.45	271.33	15.52	0.32	4.71	No data	No data
S23	HMS	SK-5	7.51	251.63	15.56	0.28	7.92	No data	No data
S24	HMS	SK-6	7.45	256.33	14.92	0.29	3.14	No data	No data
S25	HMS	SK-7	7.48	246.24	16.06	0.46	6.07	No data	No data
S26	HMS	SK-8	7.45	241.53	14.5	0.22	7.89	No data	No data
S27	HMS	SK-9	7.47	219.44	16.4	0.21	3.18	No data	No data
S28	NMS	5N-3	7.36	393.09	15.91	0.25	2.71	0.87	16752.81
S29	NMS	5N-8	7.68	291.38	18.36	0.18	6.73	0.28	20058.81
S30	NMS	5M-5	6.84	421.42	7.98	0.18	6.7	0.38	34030.78
S31	NMS	3I-1	7.11	296.93	17.07	0.24	2.76	0.92	8490.57
S32	NMS	1A-28	6.95	278.44	17.39	0.36	4.94	1.31	19670.1
S33	NMS	3I-11	6.84	293.2	18.57	0.24	2.71	2.21	3476.21
S34	NMS	1B-14	6.88	286.05	17.68	0.18	6.82	1.38	10140.85
S35	NMS	1A-22	7.48	282.71	17.03	0.18	6.87	1.13	3147.96
S36	NMS	3K-3	7.01	206.27	14.03	0.41	5.26	2.06	1869.54
S37	NMS	4G-15	7.06	268.33	16.82	0.18	6.68	0.87	77.94
S38	NMS	2E-11	6.54	290.39	16.03	0.23	2.74	0.72	1567.21
S39	NMS	3I-18	7.01	293.8	18.55	0.37	4.91	0.46	3912.43
S40	NMS	1A-1	7.12	273.16	15.44	0.18	6.78	0.55	44307.05
S41	NMS	2D-5	7.03	185.56	18.12	0.4	5.23	0.48	64217.64
S42	MMS	5M-1	6.88	250.39	17.8	0.36	4.92	0.85	2849.95
S43	MMS	6Q-23	7.05	394.55	8.76	0.25	2.69	0.55	3031.35
S44	MMS	4G-8	7.52	292.47	18.19	0.35	4.7	0.17	7086.89
S45	MMS	4G-7	5.57	289.84	18.25	0.34	4.72	0.85	17456.81
S46	HMS	3J-1	6.18	436.82	18.86	0.35	4.73	0.75	4433.16

Paddy soils were divided into three categories according to mercury concentration: NMS, non-Hg polluted soils; MMS, moderate Hg-polluted soils; HMS, high Hg-polluted soils. No data indicate that the concentrations of S^{2-} and Fe^{2+} were unavailable in soil samples from September 2020 (S1-S26).

Table S4. Key characteristics of co-occurrence networks in paddy soils.

Category	Connected nodes	Edges	Module	Average degree	Network diameter	Modularity index
NMS	199	3062	6	15.31	9	0.554
MMS	193	1655	11	8.275	7	0.583
HMS	189	1714	11	8.57	7	0.591

NMS, non-Hg polluted paddy soils (n = 23); MMS, moderate Hg-polluted paddy soils (n = 13); HMS, high Hg-polluted paddy soils (n = 10).

Table S5. Identification of major module (also known as core microbiome) in different paddy soils.

ID	Module	The number of connections to other modules	Relative abundance (%)	Correlation with MeHg concentration	Correlation with %MeHg
NMS	module1	146	34	0.418*	0.787***
	module2	13	23.5	0.164	-0.374
	module3	28	19	0.206	-0.31
	module4	3	16.5	0.189	-0.256
	module5	17	6.5	0.116	-0.186
	module6	0	0.5	0.047	-0.05
MMS	module1	66	27.5	0.503*	0.863**
	module2	84	20.5	0.035	-0.165
	module3	8	17.5	-0.103	0.066
	module4	59	9	0.068	0.051
	module5	5	8	0.206	-0.204
	module6	5	5.5	-0.049	0.106
	module7	5	3	-0.085	0.04
	module8	3	2.5	0.039	-0.065
	module9	0	2	0.101	-0.169
	module10	1	1	-0.008	0.016
	module11	0	3.5	0.026	-0.064
HMS	module1	161	20	0.410*	0.872**
	module2	120	18.5	-0.351	0.531
	module3	0	16.5	0.318	-0.518
	module4	25	9.5	-0.113	0.219
	module5	43	9	-0.259	0.654*
	module6	29	7.5	-0.302	0.518
	module7	0	5	-0.101	0.215
	module8	0	3.5	0.002	-0.008
	module9	0	1.5	-0.029	0.126
	module10	0	1.5	-0.106	0.204
	module11	0	7.5	0.284	-0.579

NMS, non-Hg polluted paddy soils (n = 23); MMS, moderate Hg-polluted paddy soils (n = 13); HMS, high Hg-polluted paddy soils (n = 10).

References:

Cline, J. D.: Spectrophotometric determination of hydrogen sulfide in natural waters1, Limnol. Oceanogr., 14, 454-458, https://doi.org/10.4319/lo.1969.14.3.0454, 1969.

EPA, U.: Method 1630: Methyl Mercury in Water by Distillation, Aqueous Ethylation, Purge and Trap, and Cold Vapor Atomic Fluorescence Spectrometry CVAFS (EPA-821-R-01-020), United States Environmental Protection Agency, Washington, DC, https://www.epa.gov/sites/default/files/2015-08/documents/method_1630_1998.pdf, 2001.

EPA, U.: Method 1631, Revision E: Mercury in Water by Oxidation, Purge and Trap, and Cold Vapor Atomic Fluorescence Spectrometry (EPA-821-R-02-019), United States Environmental Protection Agency, Washington, DC, https://www.epa.gov/sites/default/files/2015-08/documents/method_1631e_2002.pdf, 2002.

Hu, H., Lin, H., Zheng, W., Tomanicek, S. J., Johs, A., Feng, X., Elias, D. A., Liang, L., and Gu, B.: Oxidation and methylation of dissolved elemental mercury by anaerobic bacteria, Nat. Geosci., 6, 751-754, https://doi.org/10.1038/ngeo1894, 2013.

Jiang, T., Bravo, A. G., Skyllberg, U., Björn, E., Wang, D. Y., Yan, H., and Green, N. W.: Influence of dissolved organic matter (DOM) characteristics on dissolved mercury (Hg) species composition in sediment porewater of lakes from southwest China, Water Res., 146, 146-158, https://doi.org/10.1016/j.watres.2018.08.054, 2018.

Liu, J., Zhao, L., Kong, K., Abdelhafiz, M. A., Tian, S., Jiang, T., Meng, B. and Feng, X.: Uncovering geochemical fractionation of the newly deposited Hg in paddy soil using a stable isotope tracer, J. Hazard. Mater., 433, 128752-128752, https://doi.org/10.1016/j.jhazmat.2022.128752, 2022.

Liu, Y., Johs, A., Li, B., Lu, X., Hu, H., Sun, D. H., He, J. Z., and Gu, B.: Unraveling Microbial Communities Associated with Methylmercury Production in Paddy Soils, Environ. Sci. Technol., 52, 13110-13118, https://doi.org/10.1021/acs.est.8b03052, 2018.

Shi, J. B., Liang, L. N., Jiang, G. B. and Jin, X. L.: The speciation and bioavailability of mercury in sediments of Haihe River, China, Environ. Int., 31, 357-365, https://doi.org/10.1016/j.envint.2004.08.008, 2005.

van Hees, P. A. W., Dahlén, J., Lundström, U. S., Borén, H. and Allard, B.: Determination of low molecular weight organic acids in soil solution by HPLC, Talanta, 48, 173-179, https://doi.org/10.1016/S0039-9140(98)00236-7, 1999.

Viollier, E., Inglett, P. W., Hunter, K., Roychoudhury, A. N. and Van Cappellen, P.: The ferrozine method revisited: Fe(II)/Fe(III) determination in natural waters, Appl. Geochem., 15, 785-790, https://doi.org/10.1016/S0883-2927(99)00097-9, 2000.

Zhang, S., Yin, Y., Yang, P., Yao, C., Tian, S., Lei, P., Jiang, T. and Wang, D.: Using the end-member mixing model to evaluate biogeochemical reactivities of dissolved organic matter (DOM): autochthonous versus allochthonous origins, Water Res., 232, 119644, https://doi.org/10.1016/j.watres.2023.119644, 2023.